Dissecting the Baryon Cycle and ISM Properties with JWST NIRISS and NIRSpec Spectroscopy

Xin Wang

Collaborators: **Xianlong He**, **Sijia Li**, Cheng Cheng, Junqiang Ge, Haojing Yan, +GLASS team

UCAS/NAOC/BNU

Collaboration Workshop on Cosmology and Galaxy Formation @ SJTU

Jun 20, 2023

Baryon Cycle (in the eyes of an artist)

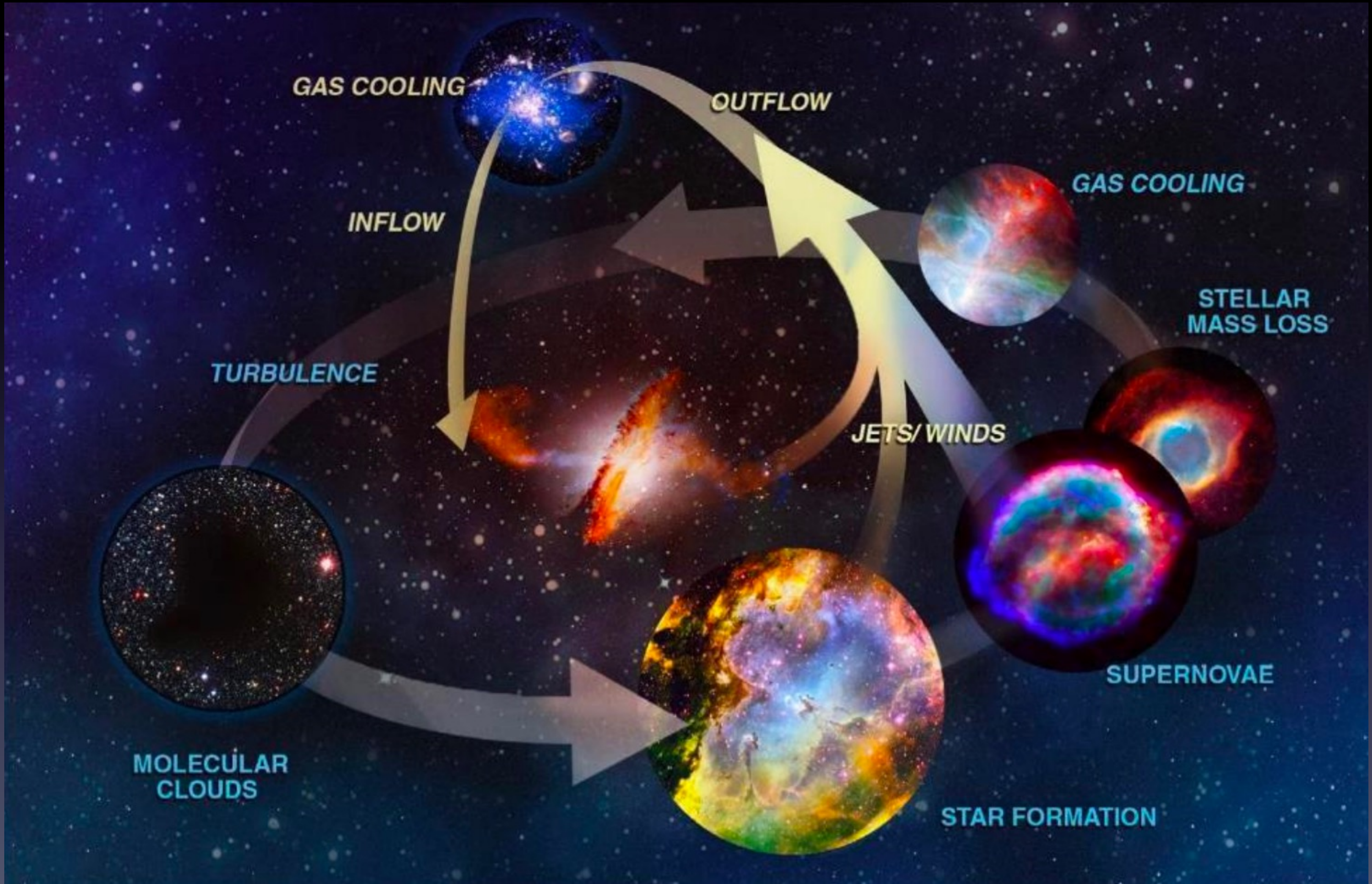

Baryon Cycle (in the eyes of an astrophysicist)

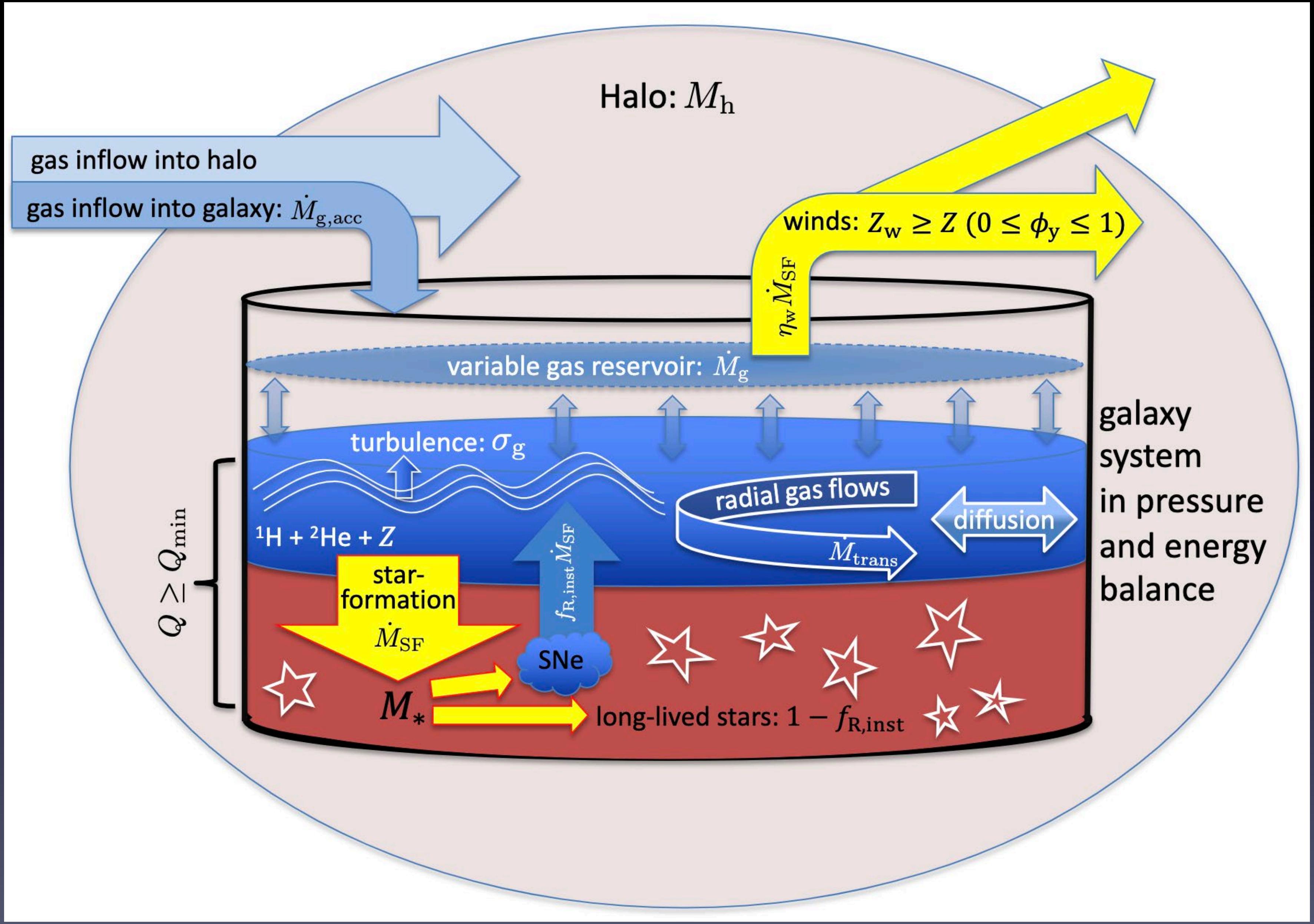

The **bathtub model** of galaxy chemical evolution (Bouche et al. 2010, Finlator & Dave 2008; Recchi et al. 2008; Dave, Finlator & Oppenheimer 2012; Dayal, Ferrara & Dunlop 2013; Dekel et al. 2013; Lilly et al. 2013; Pipino, Lilly & Carollo 2014; Dekel & Mandelker 2014; Peng & Maiolino 2014; Sharda et al. 2023)

Baryon Cycle

↑

Interstellar Medium (ISM)

Chemical Evolution ↕ Galactic feedback

Stellar Evolution

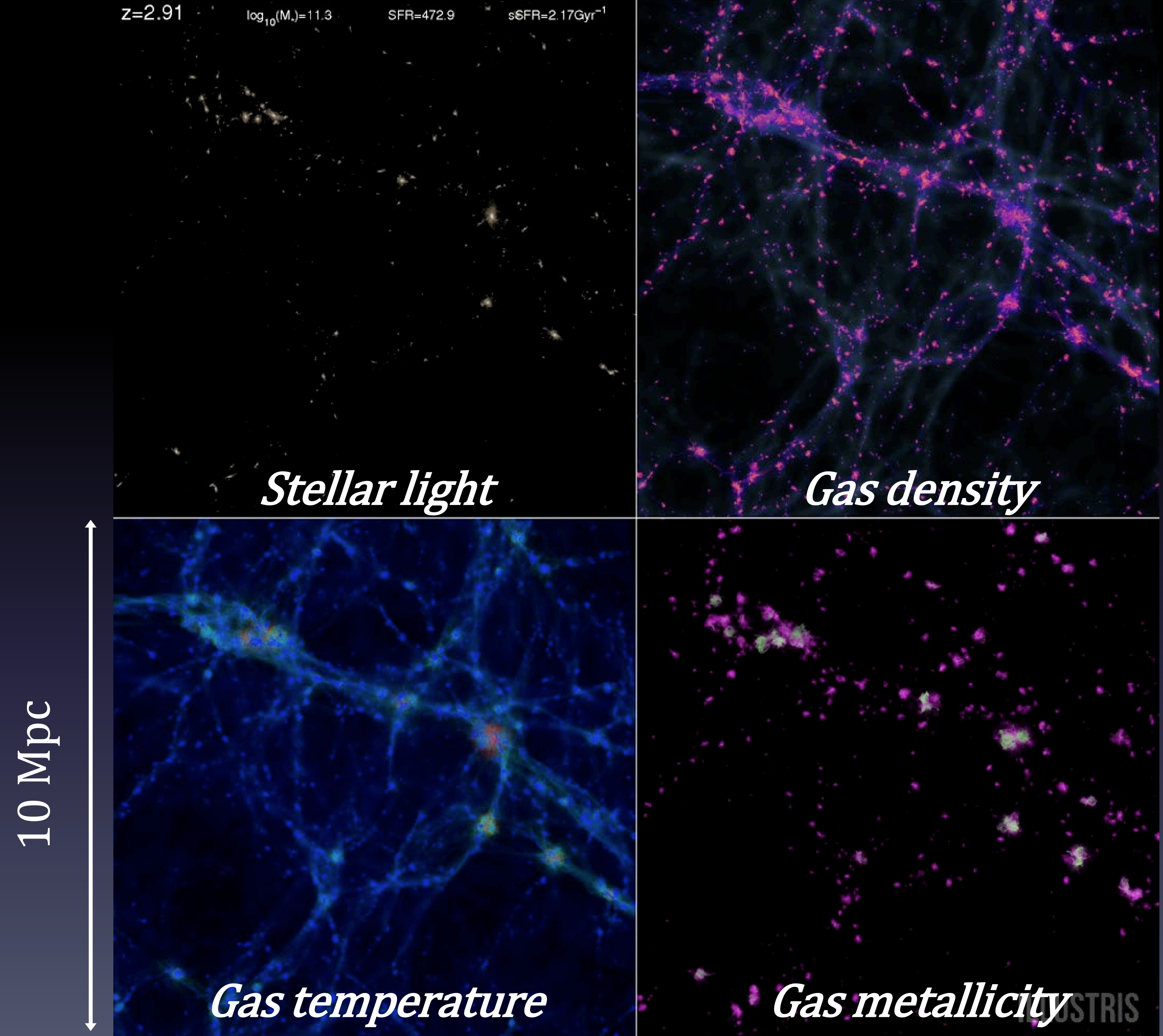

Baryon Cycle

↑

Interstellar Medium (ISM)

↕ Chemical Evolution — Galactic feedback

Stellar Evolution

10 Mpc

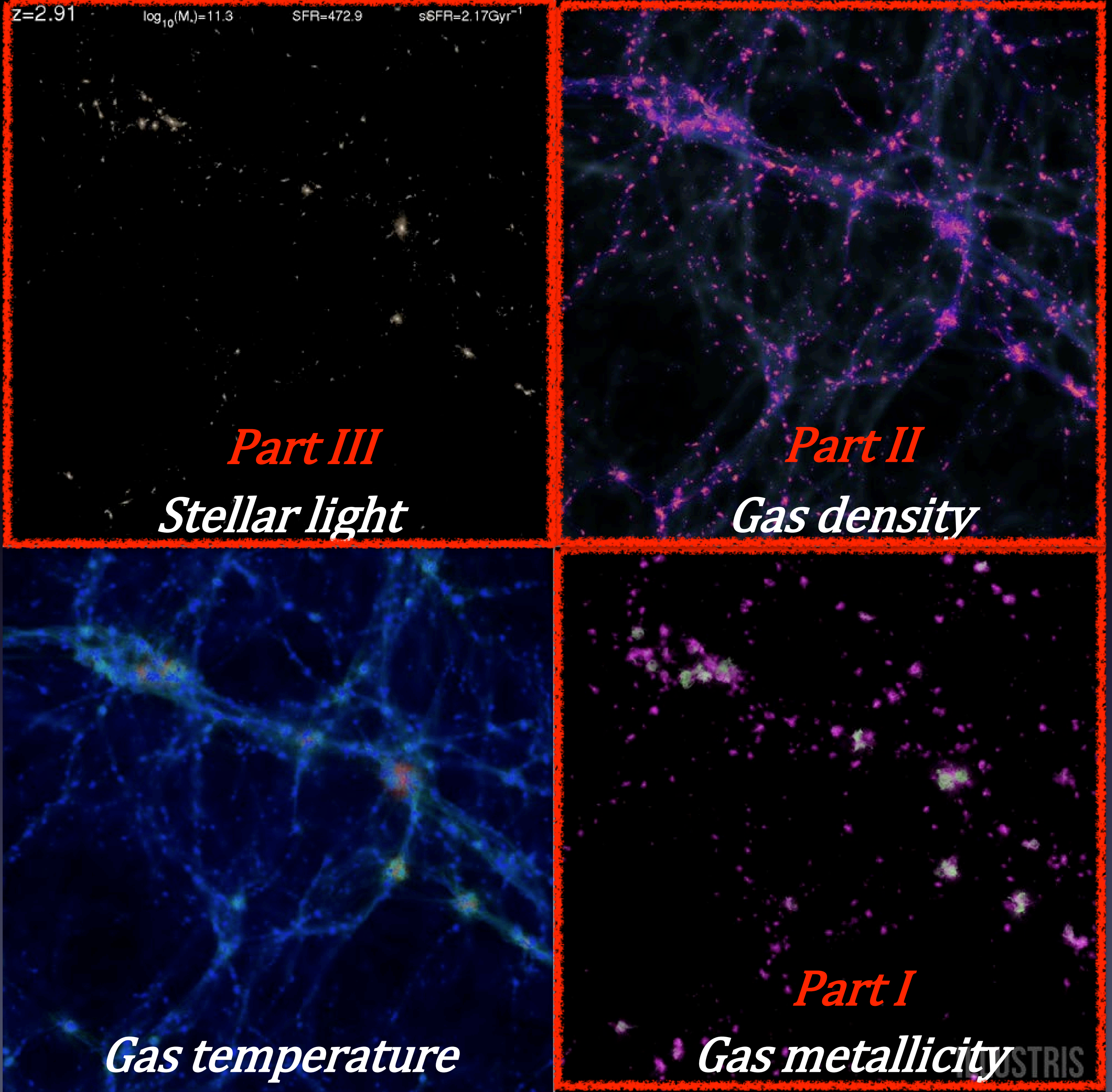

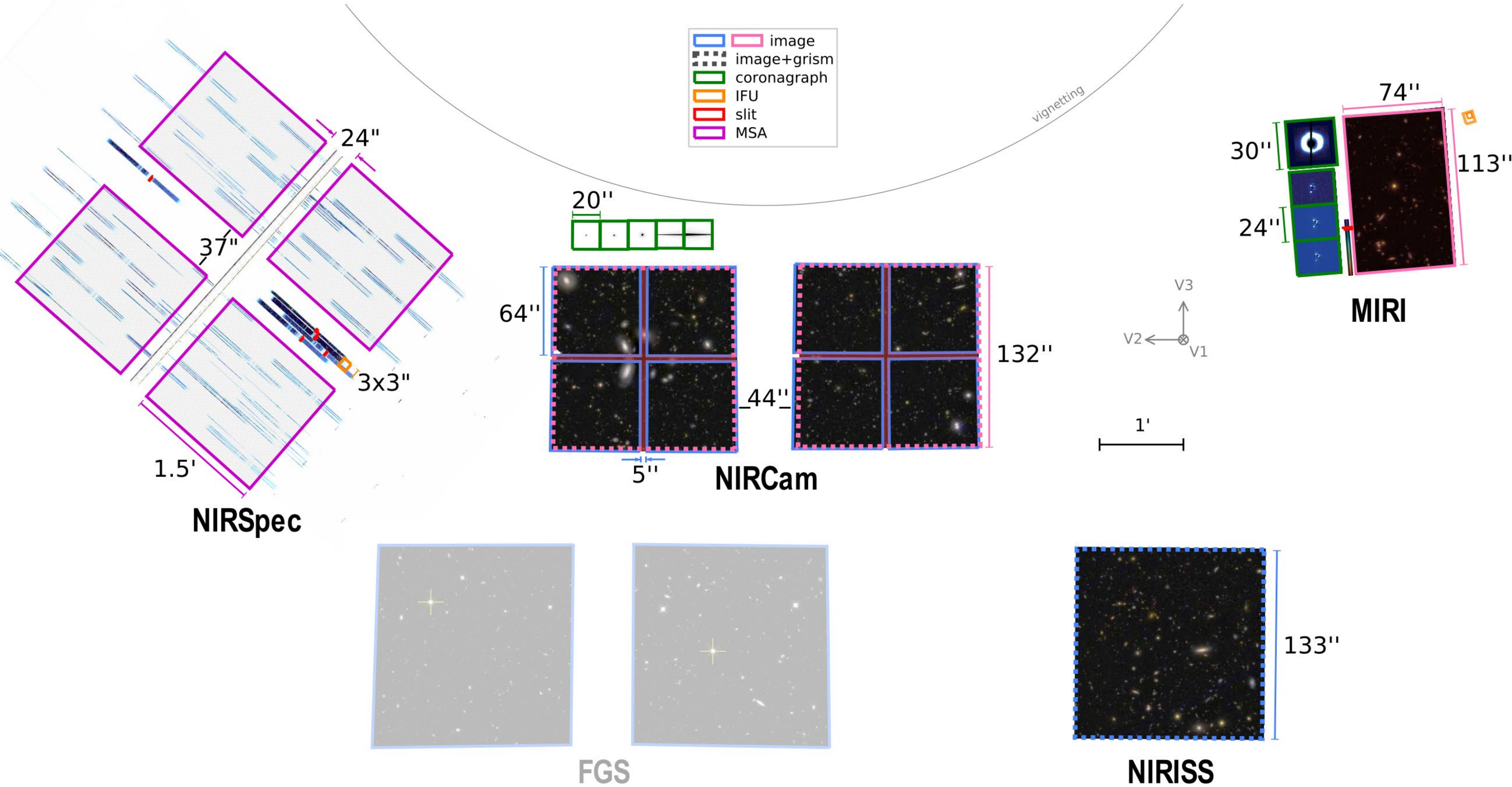

image
image+grism
coronagraph
IFU
slit
MSA
vignetting
24"
37"
3x3"
1.5'
NIRSpec
20''
64''
44''
132''
5''
NIRCam
74''
30''
113''
24''
MIRI
V3
V2
V1
1'
FGS
133''
NIRISS

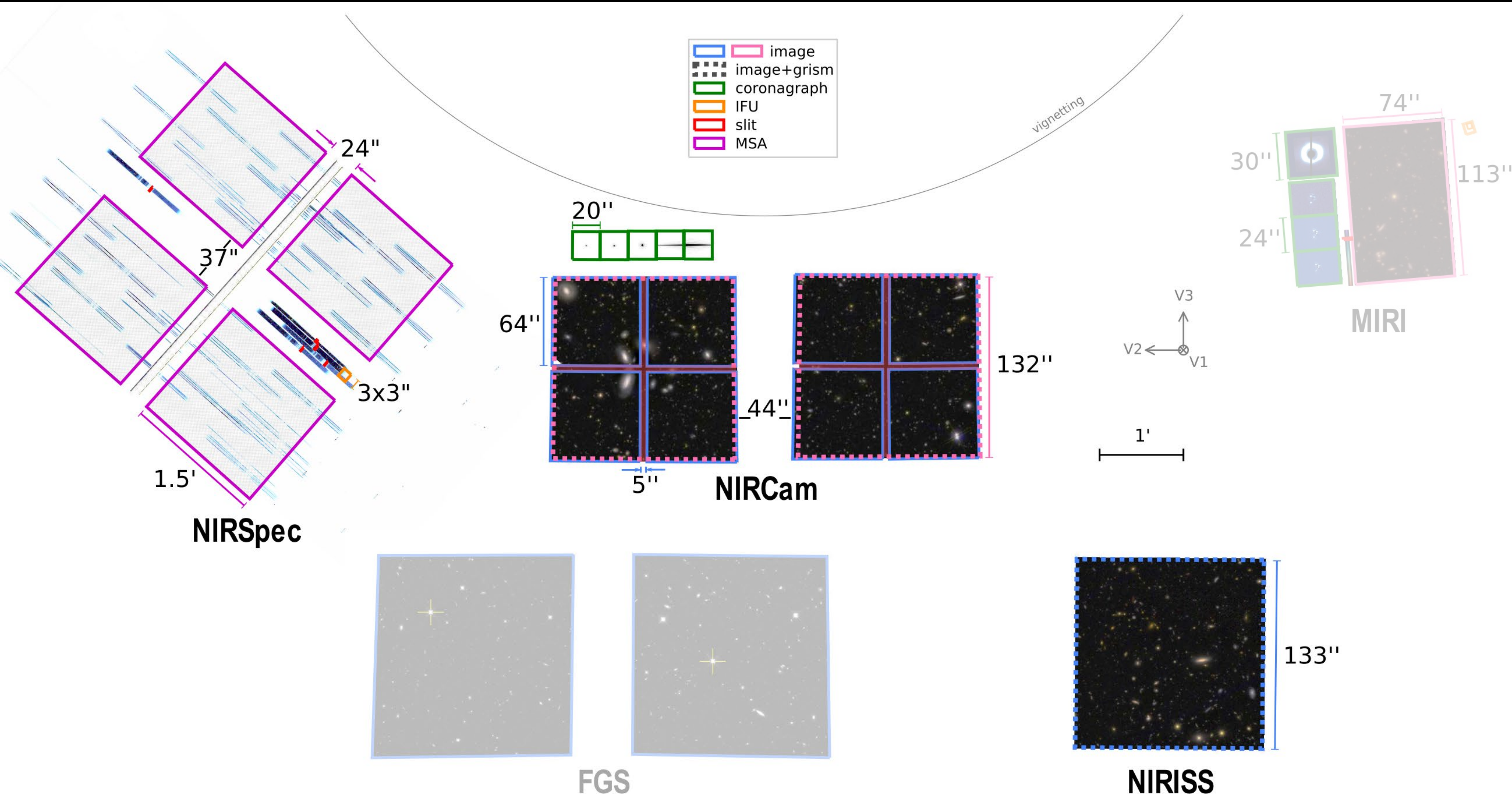

image
image+grism
coronagraph
IFU
slit
MSA
vignetting
24"
37"
3x3"
1.5'
NIRSpec
20''
64''
44''
5''
132''
NIRCam
74''
30''
113''
24''
MIRI
V3
V2
V1
1'
FGS
133''
NIRISS

Primary Target and Observing Modes

- NIRISS Wide Field Slitless Spectroscopy R~150 (F115, F150W, F200W): 35ks
- Parallel NIRCAM imaging (F090W, F115W, F150W, F277W, F200W, F356W, F444W) 30ks; mAB~29
- NIRSPEC MOS R~2700 (F100LP, F170LP, F290LP): 52ks
- Parallel NIRCAM imaging (F090W, F115W, F150W, F277W, F200W, F356W, F444W) 50ks; mAB~29.4

GLASS-JWST

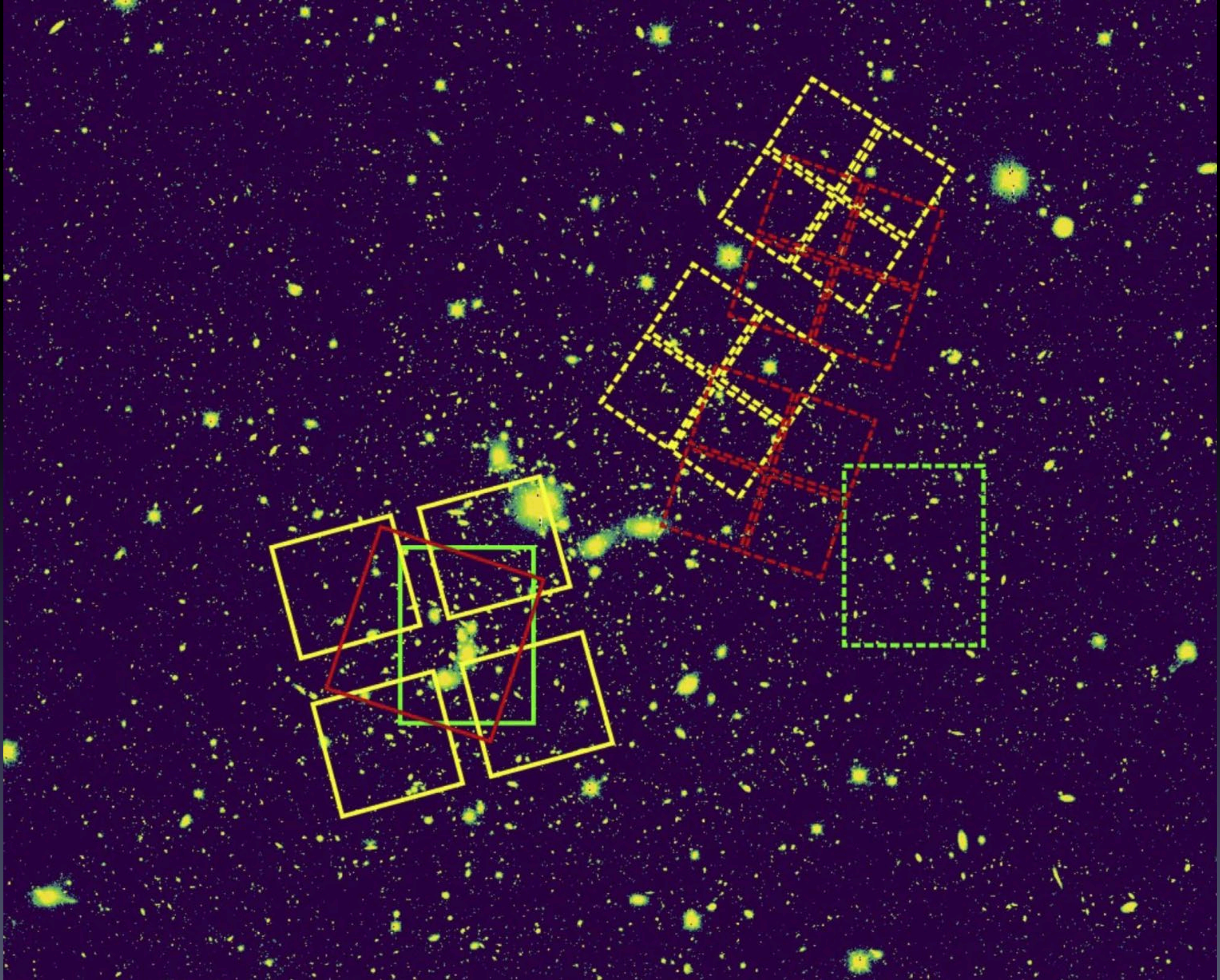

JWST and HST footprints in the Abell 2744 galaxy cluster field:

- solid: primary, dashed: coordinated parallel
- **red**: epoch 1 of GLASS-JWST. primary: NIRISS WFSS, parallel: NIRCam imaging
- **yellow**: epoch 2 of GLASS-JWST. primary: NIRSpec MSA, parallel: NIRCam imaging
- **green**: Hubble Frontier Field deep imaging

Treu et al. (2022)

JWST/NIRISS Slitless Spectroscopy of Abell 2744

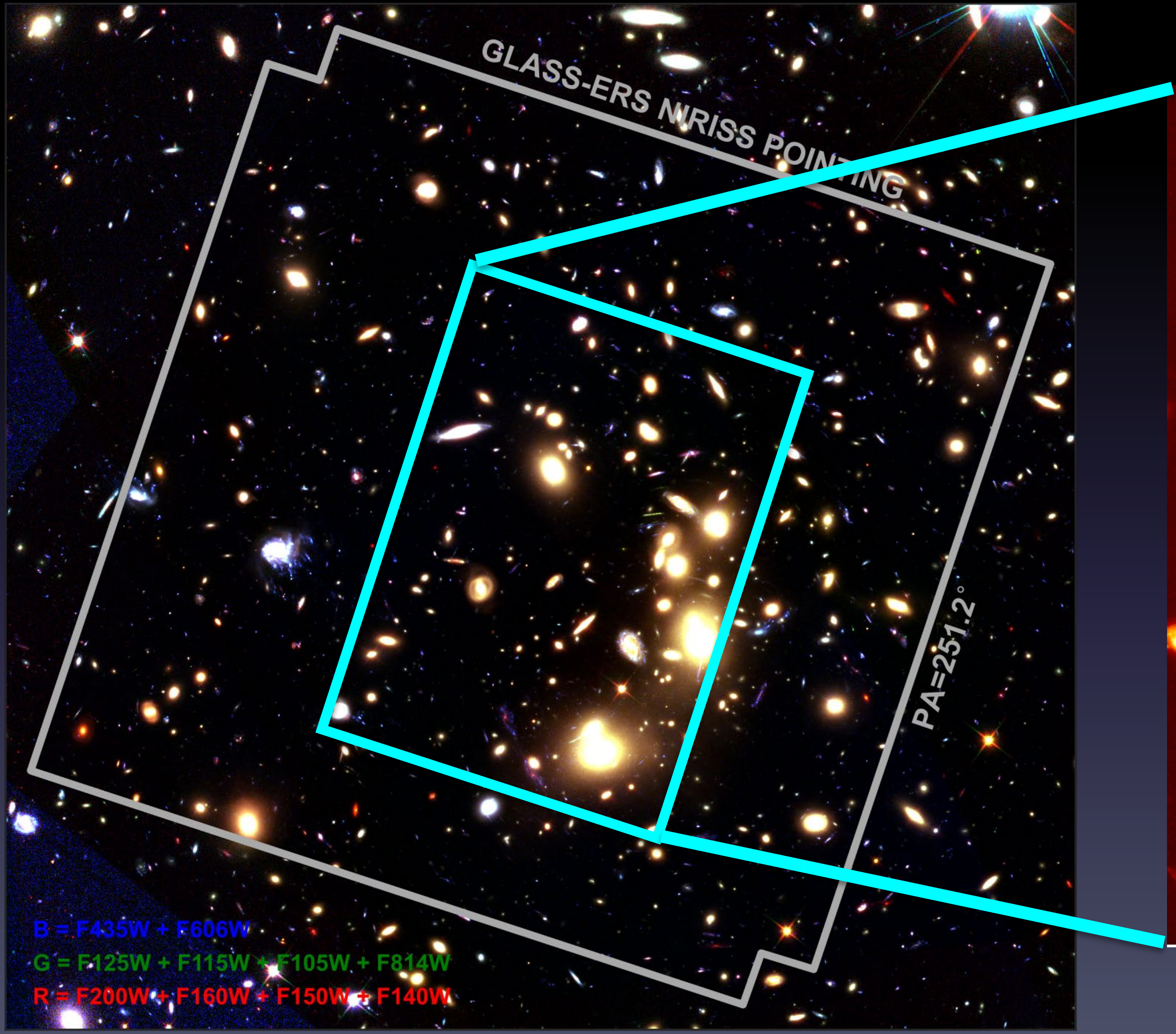

Based on JWST-ERS-1324, PI: Treu

JWST/NIRISS Slitless Spectroscopy of Abell 2744

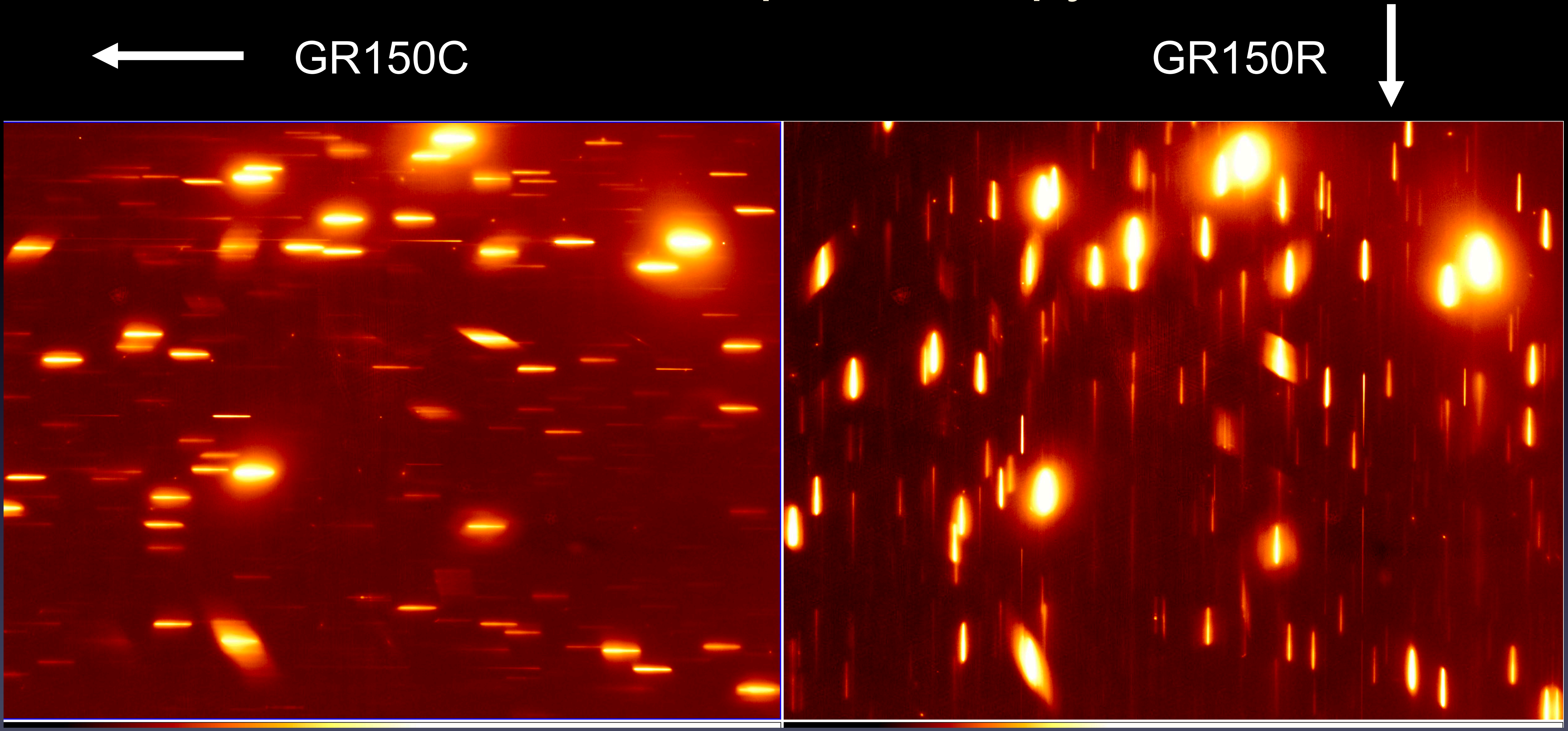

Based on JWST-ERS-1324, PI: Treu

F115W GR150C

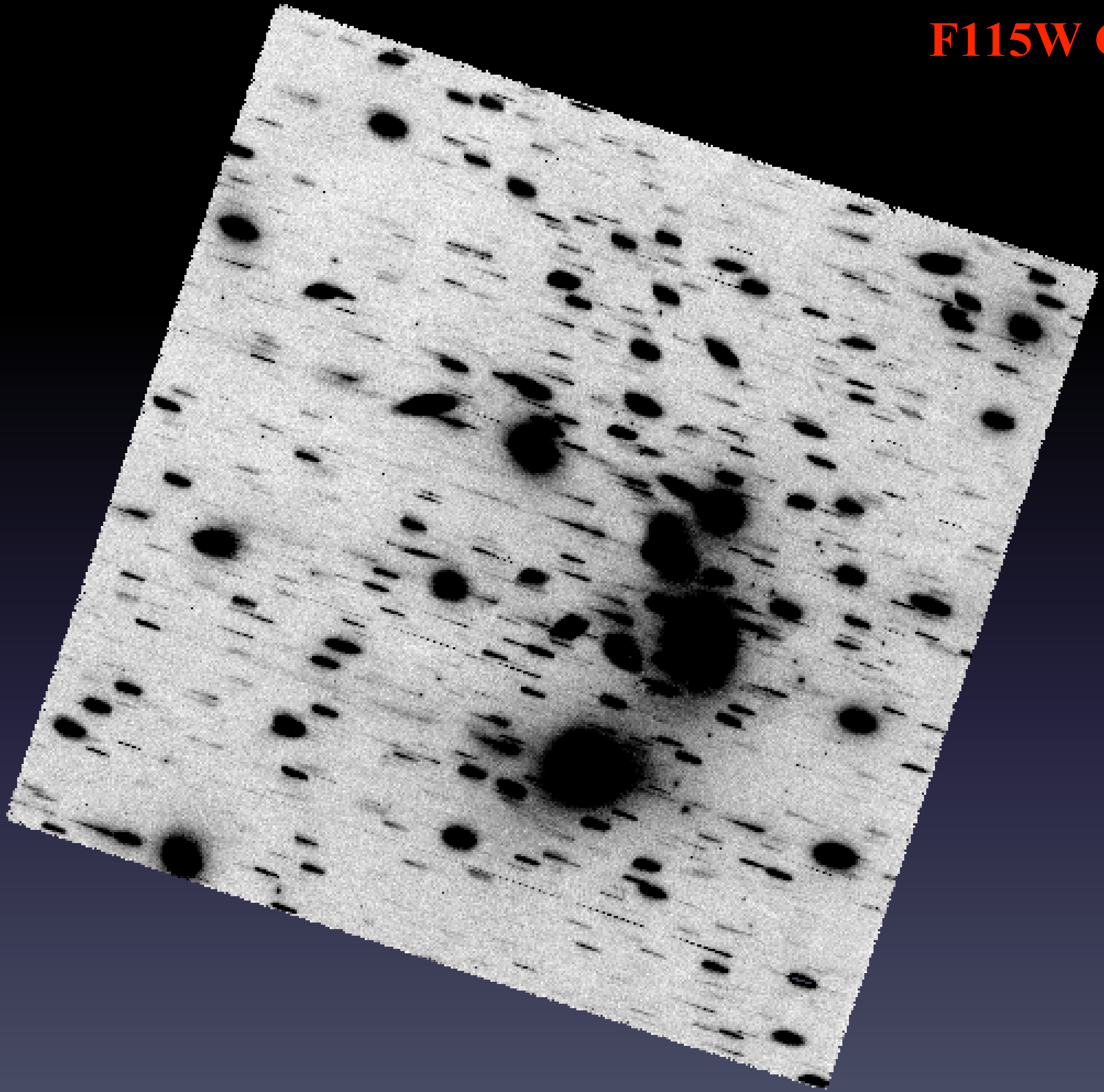

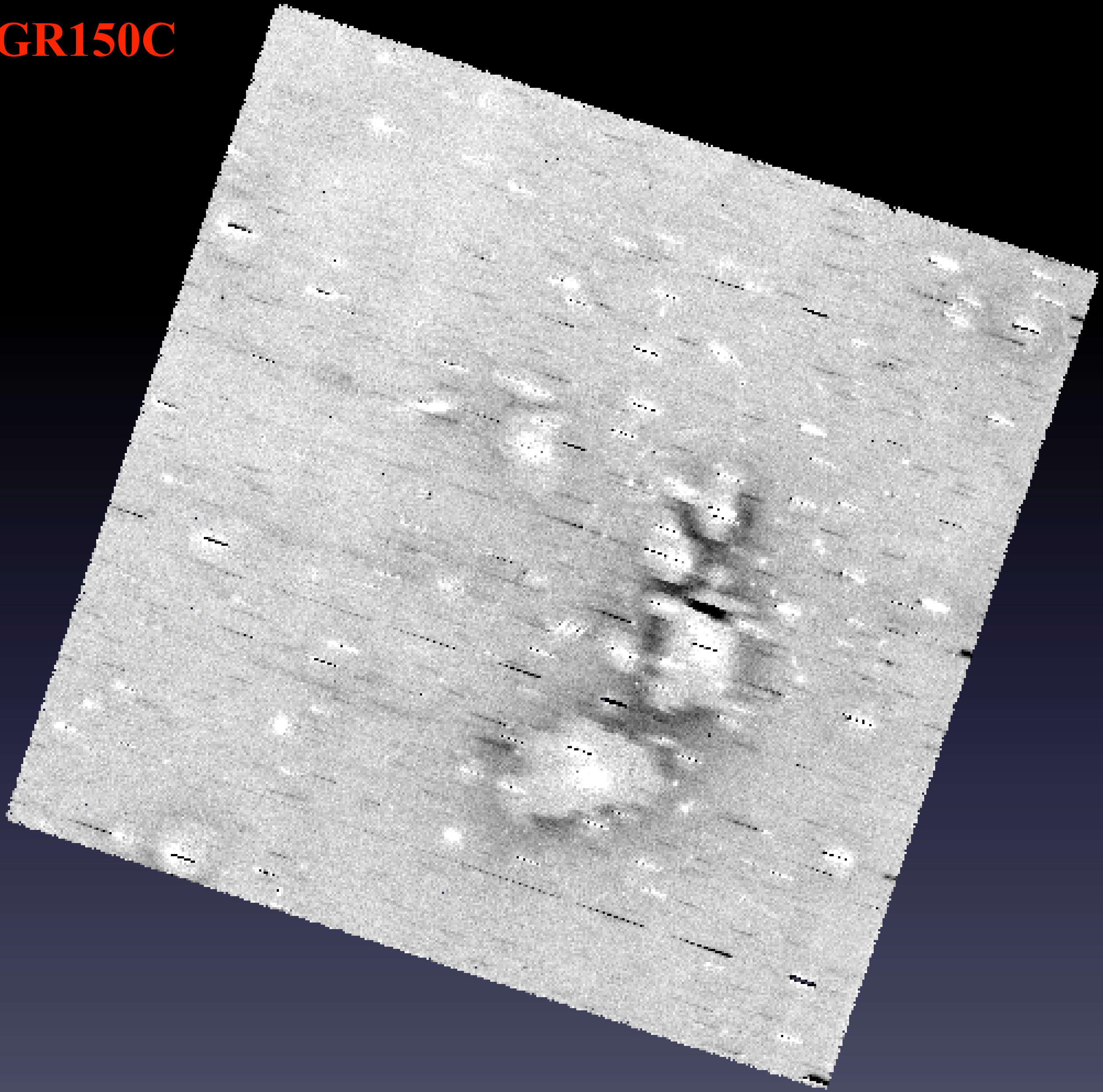

F115W GR150R

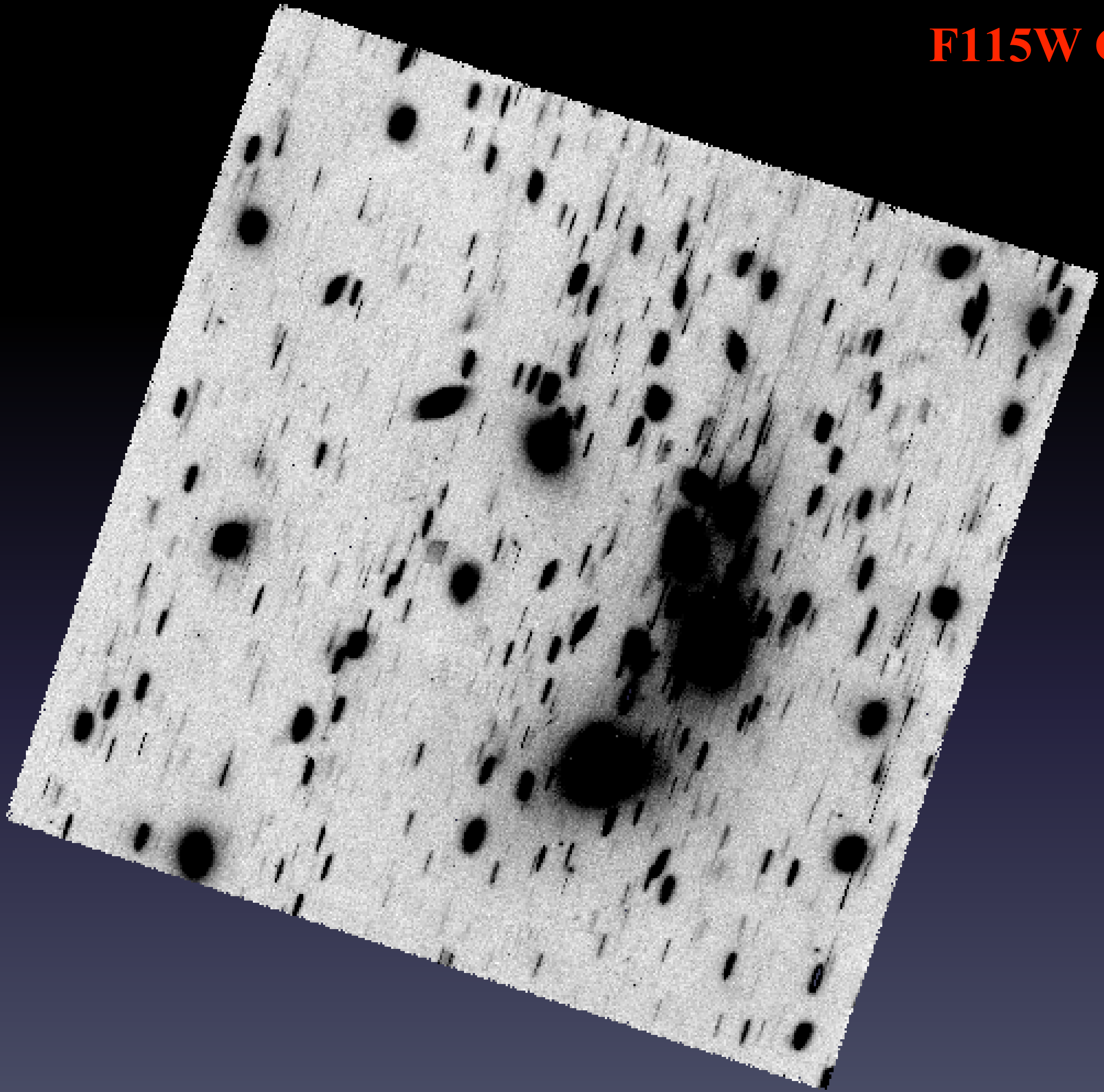

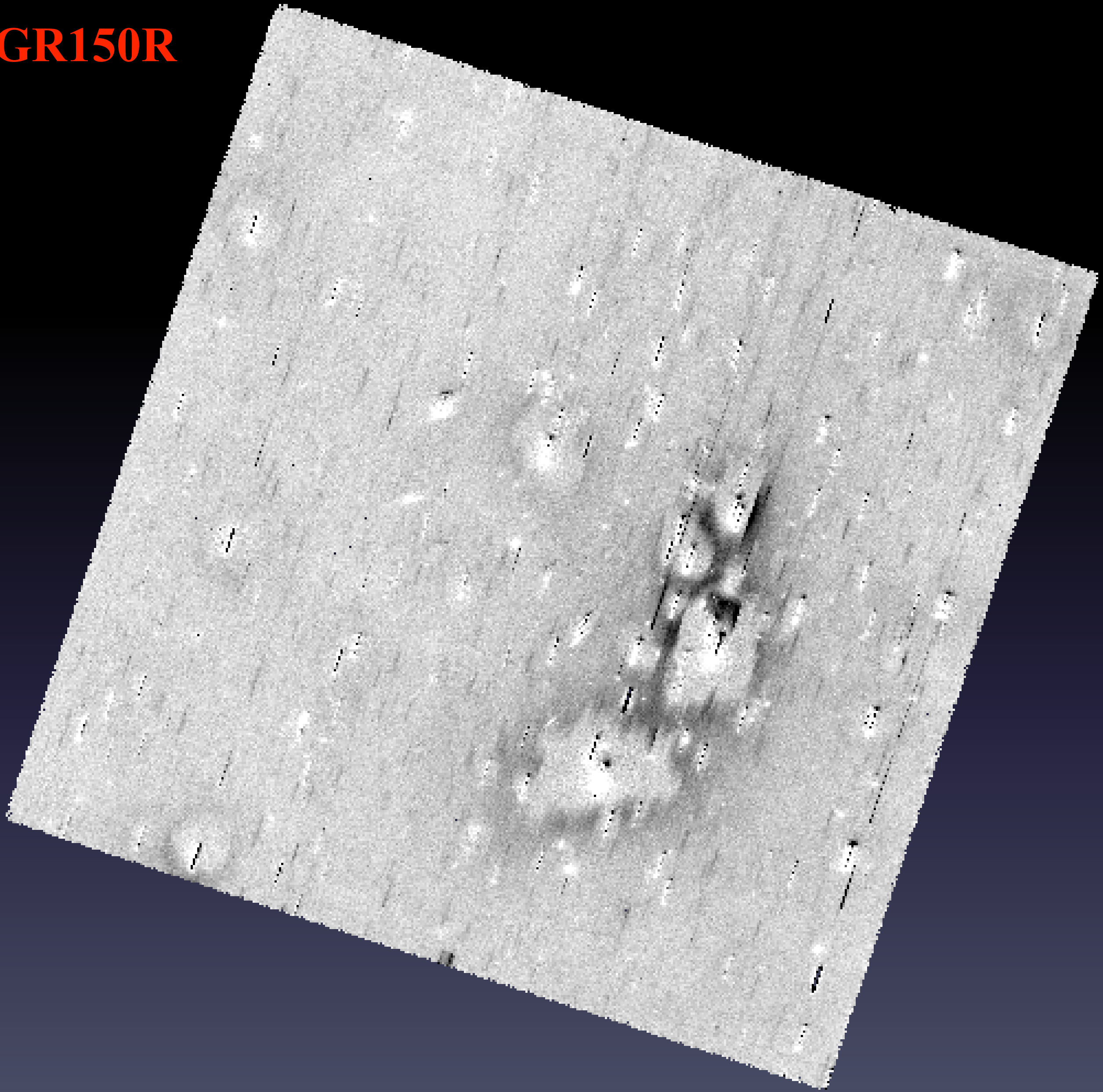

Example spectral extractions by Grizli

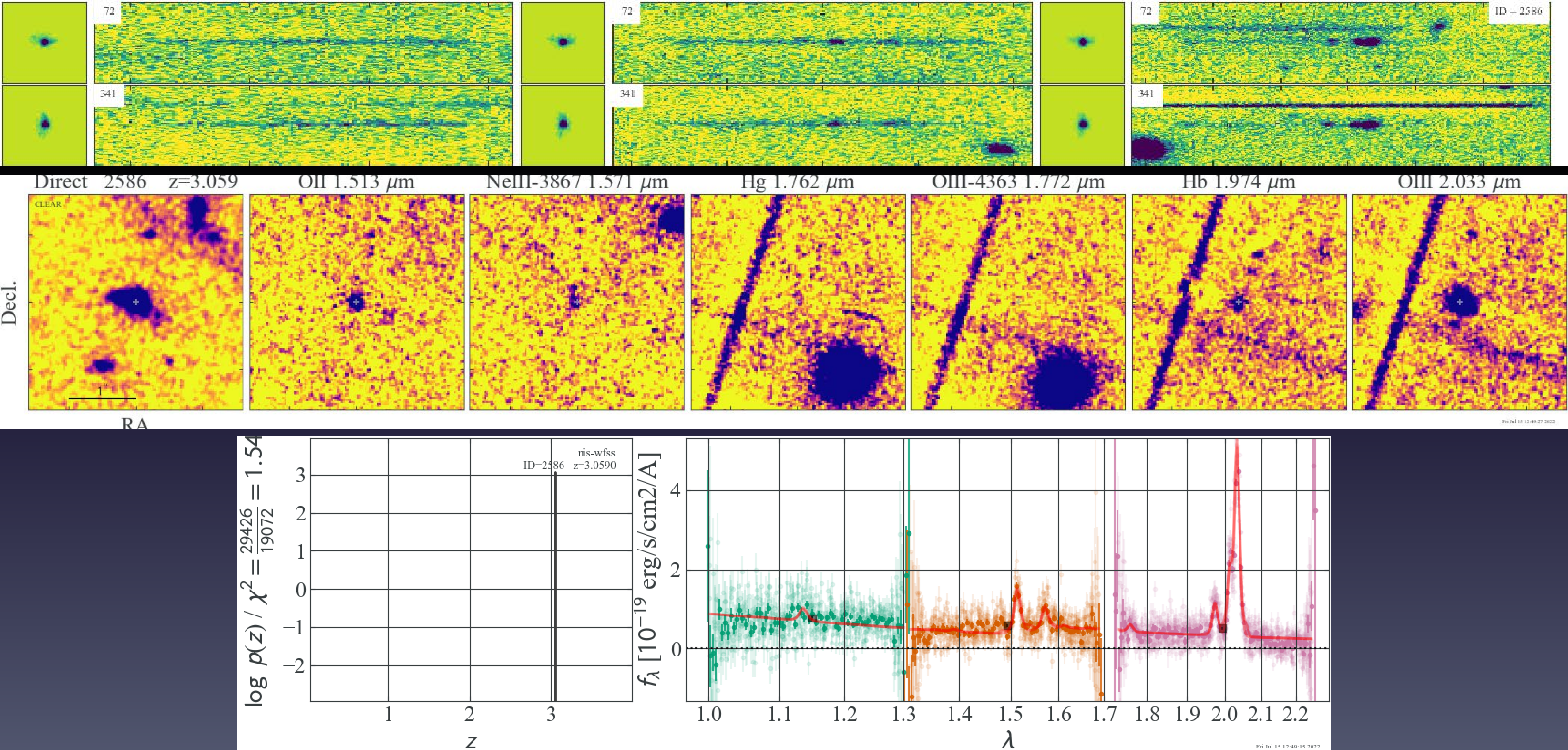

The first spatially resolved analysis from JWST grisms

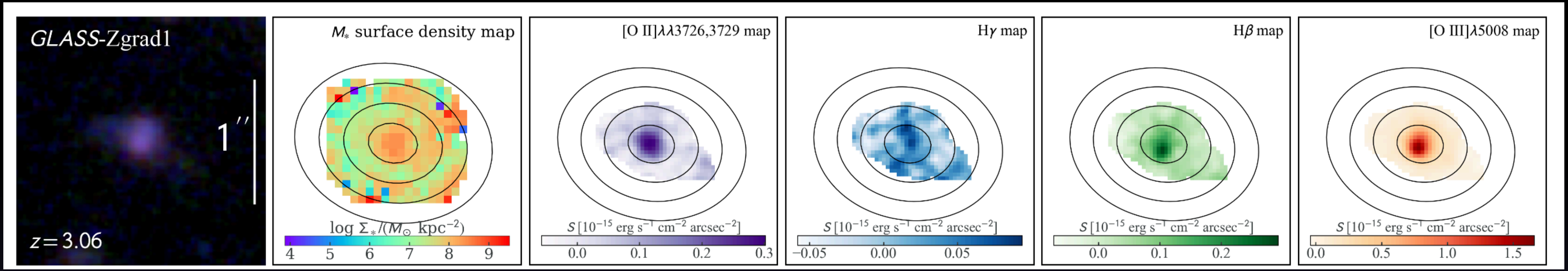

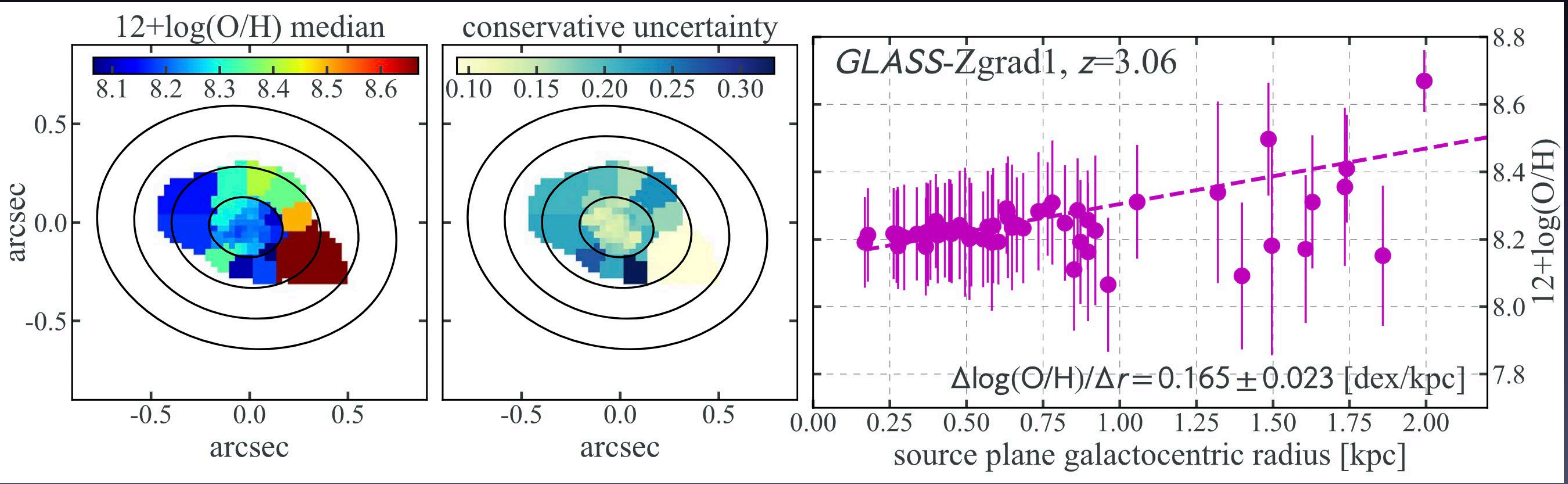

Wang et al. (2022a) arXiv:2207.13113

The first metal gradient with sub-kpc resolution at z≥3

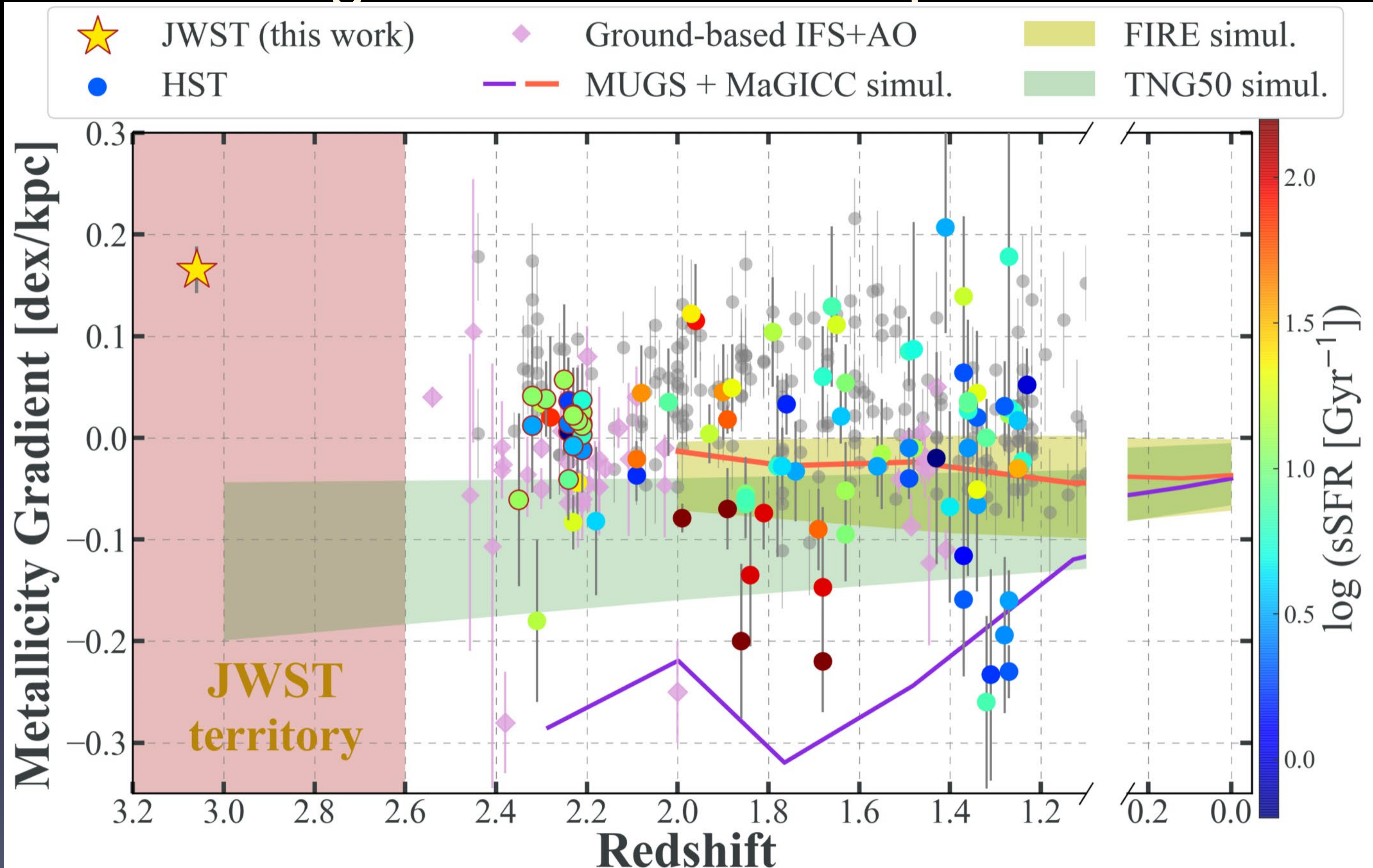

Wang et al. (2022a) arXiv:2207.13113

Spectral stacking analysis of 1D grism spectra

- Stacking the optimally extracted 1D spectra of multiple sources within the same stellar mass bin to achieve higher SNR
- Measure the correlation at the population level

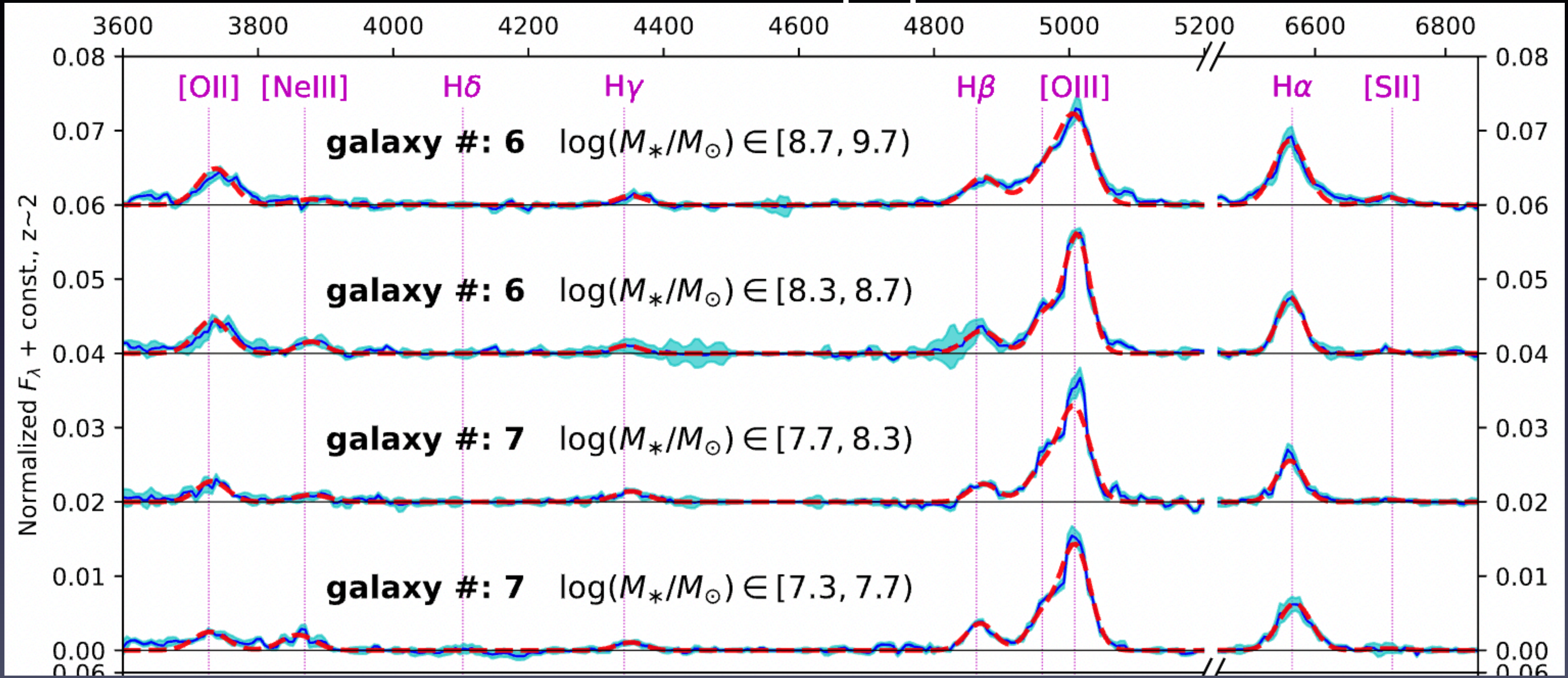

He Xianlong, **XW** et al. in prep

The mass-metallicity relation at high redshifts

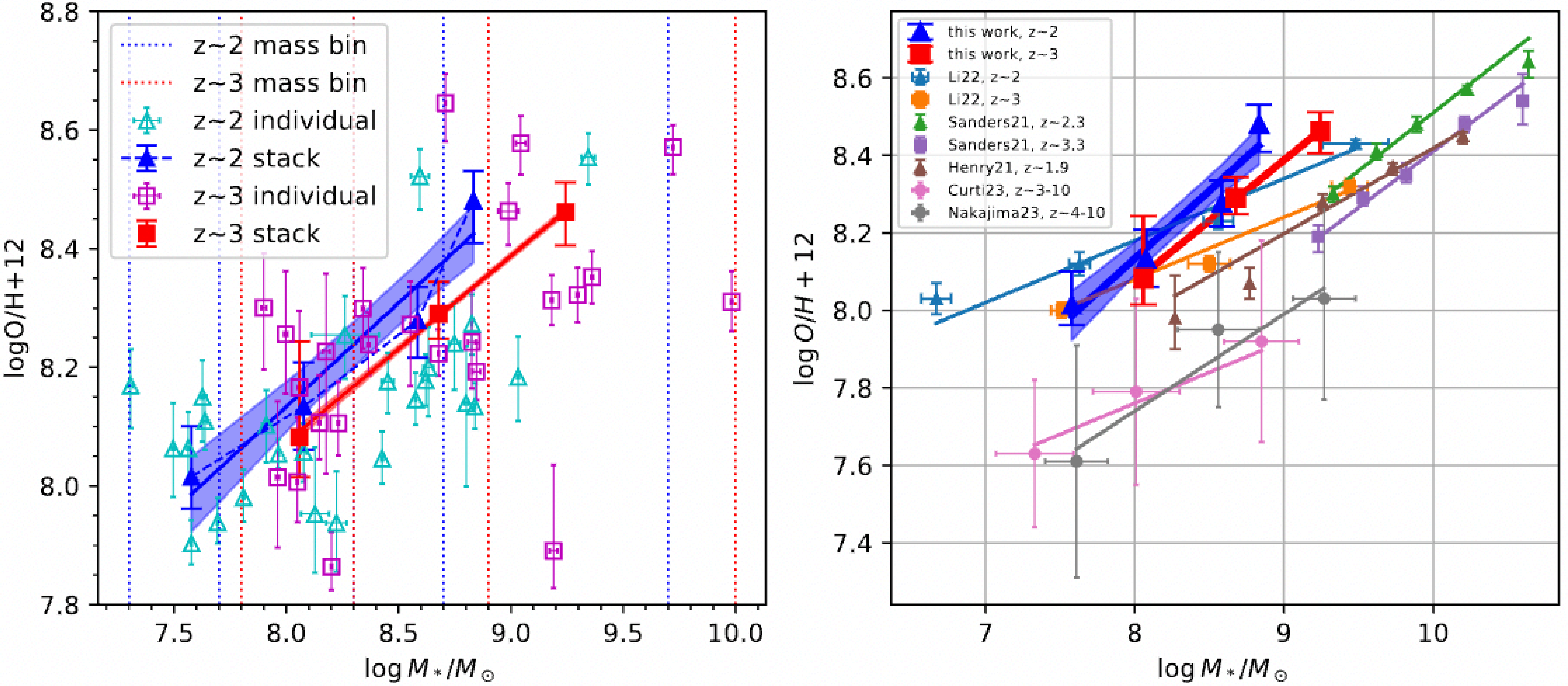

The mass-metallicity relation at high redshifts

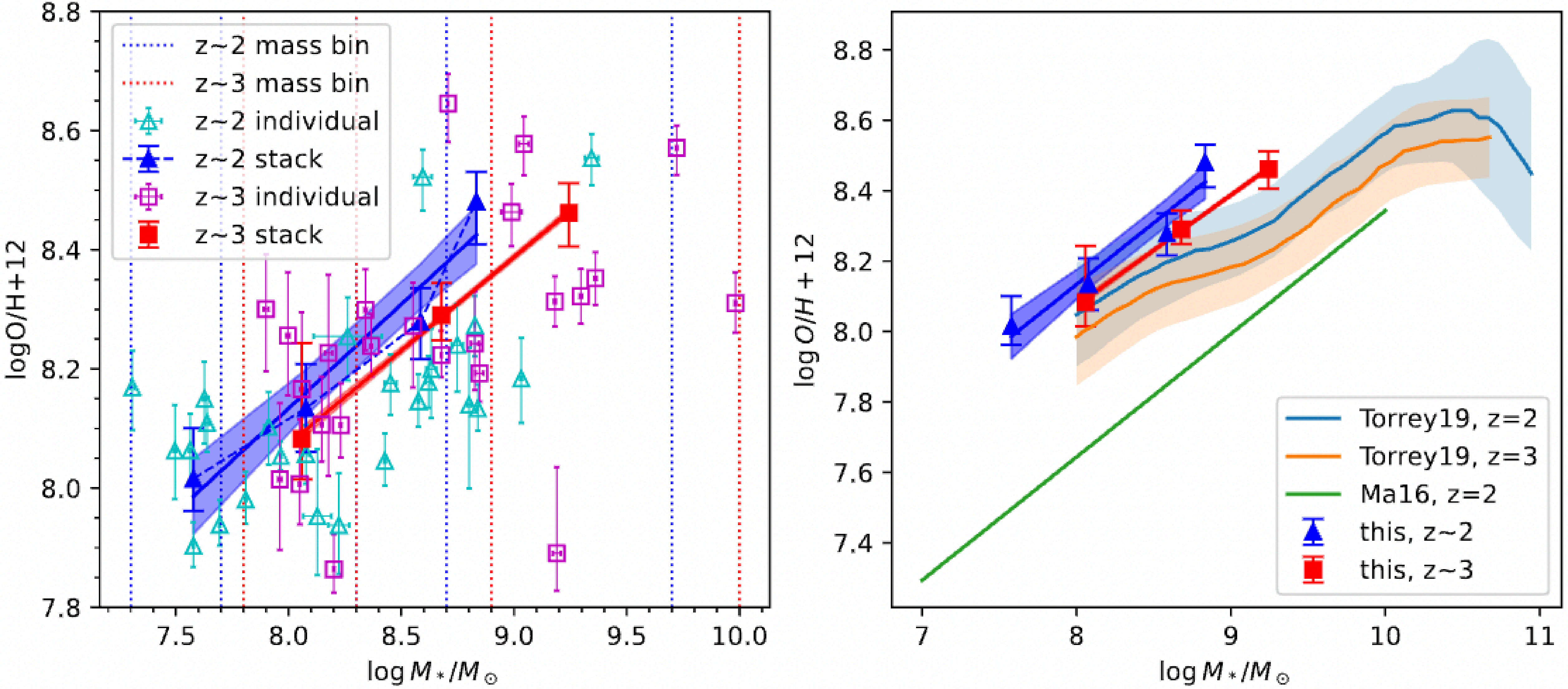

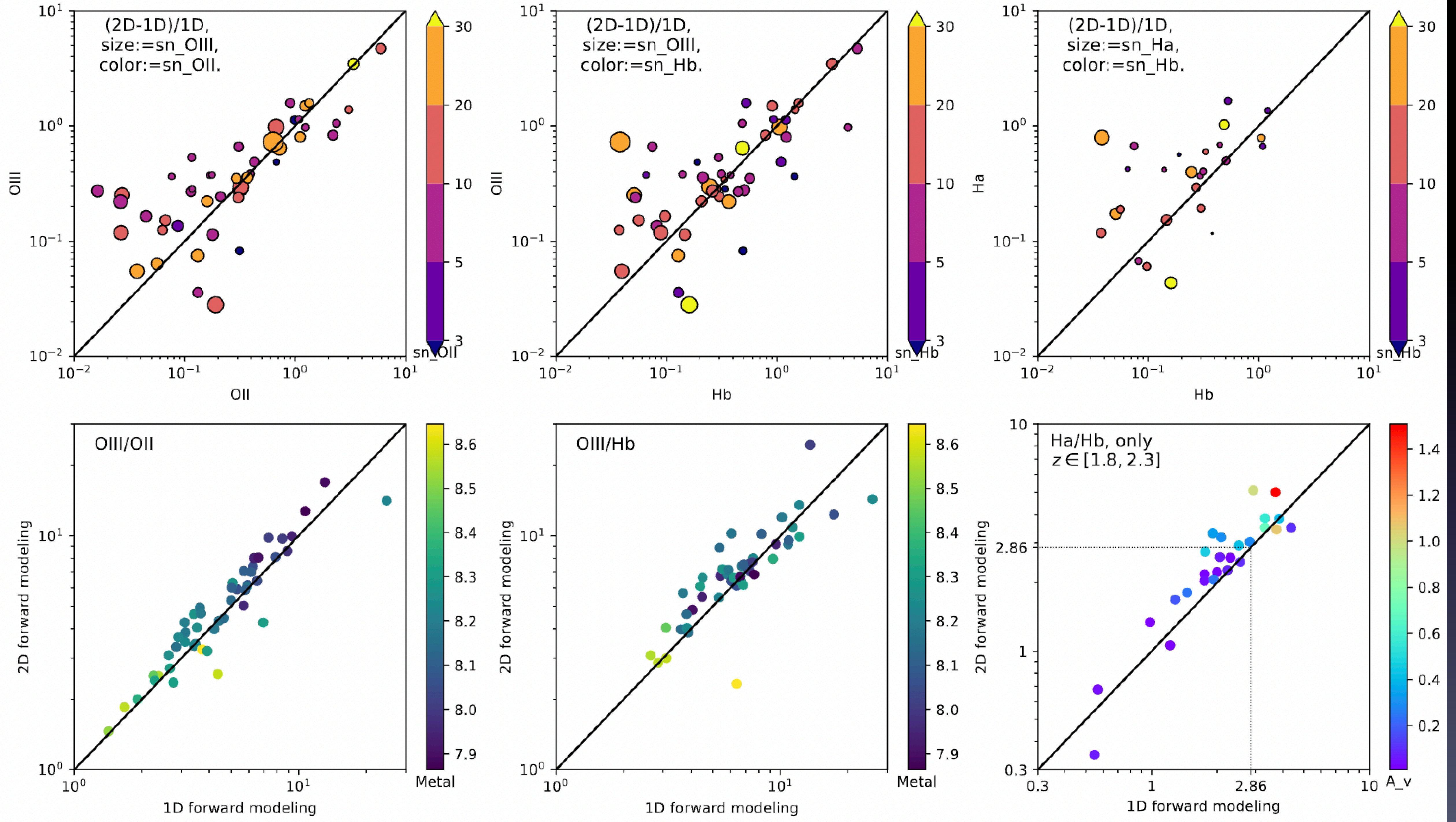
(2D-1D)/1D,
size:=sn_OIII,
color:=sn_OII.
OII
OIII
sn_OII
(2D-1D)/1D,
size:=sn_OIII,
color:=sn_Hb.
Hb
OIII
sn_Hb
(2D-1D)/1D,
size:=sn_Ha,
color:=sn_Hb.
Hb
Ha
sn_Hb
OIII/OII
OIII/Hb
Ha/Hb, only
$z \in [1.8, 2.3]$
1D forward modeling
2D forward modeling
Metal
A_v
2.86

ISM density measurements from NIRSpec Spectroscopy

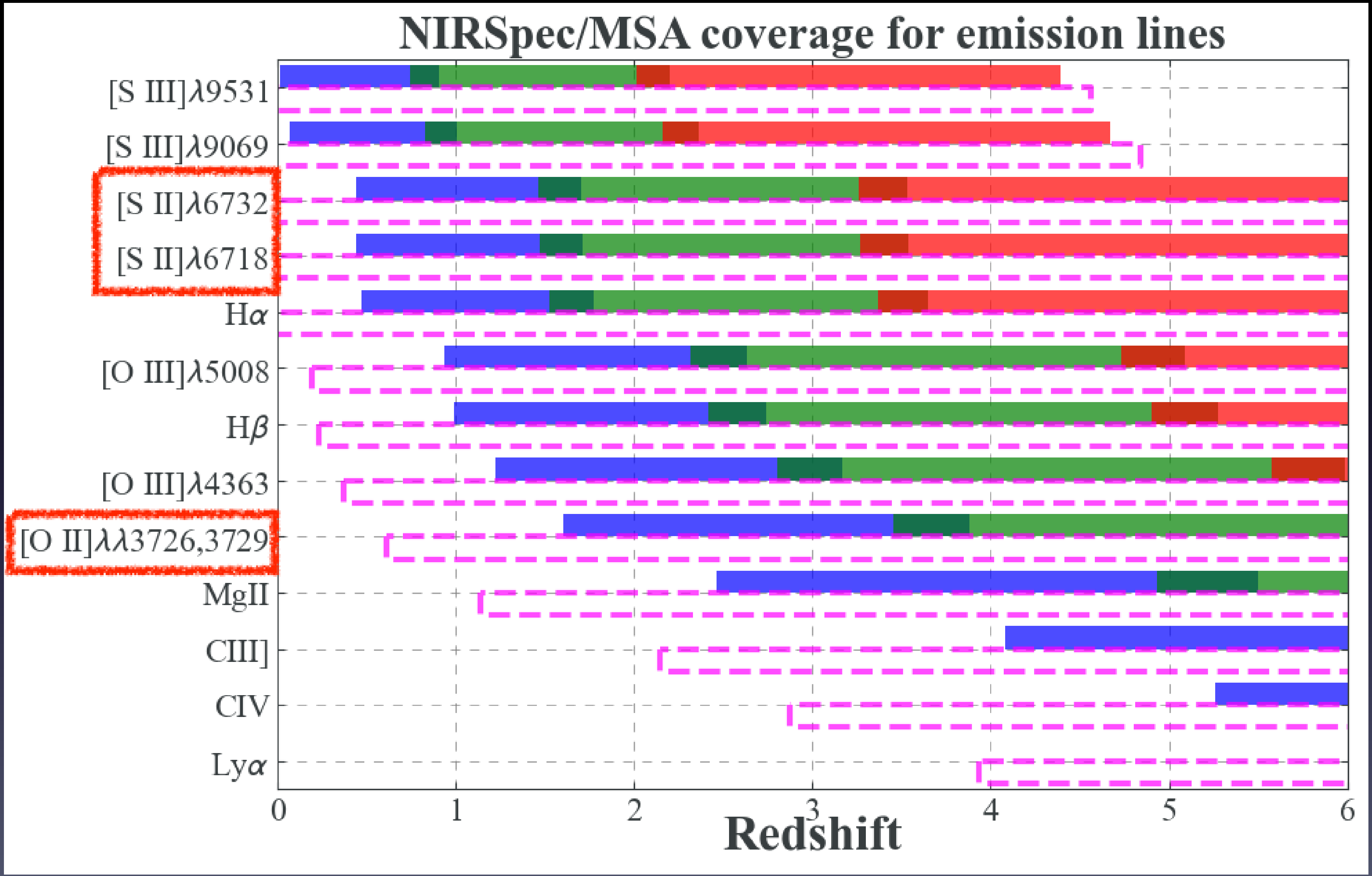

ISM density measurements from NIRSpec Spectroscopy

- ISM electron density (n_e) can be probed by the flux ratios of the line doublets of [OII]$\lambda\lambda$3727,3730 and [SII]$\lambda\lambda$6718,6732
- Isobe et al. (2022) measured n_e using OII doublets from high/medium resolution NIRSpec data

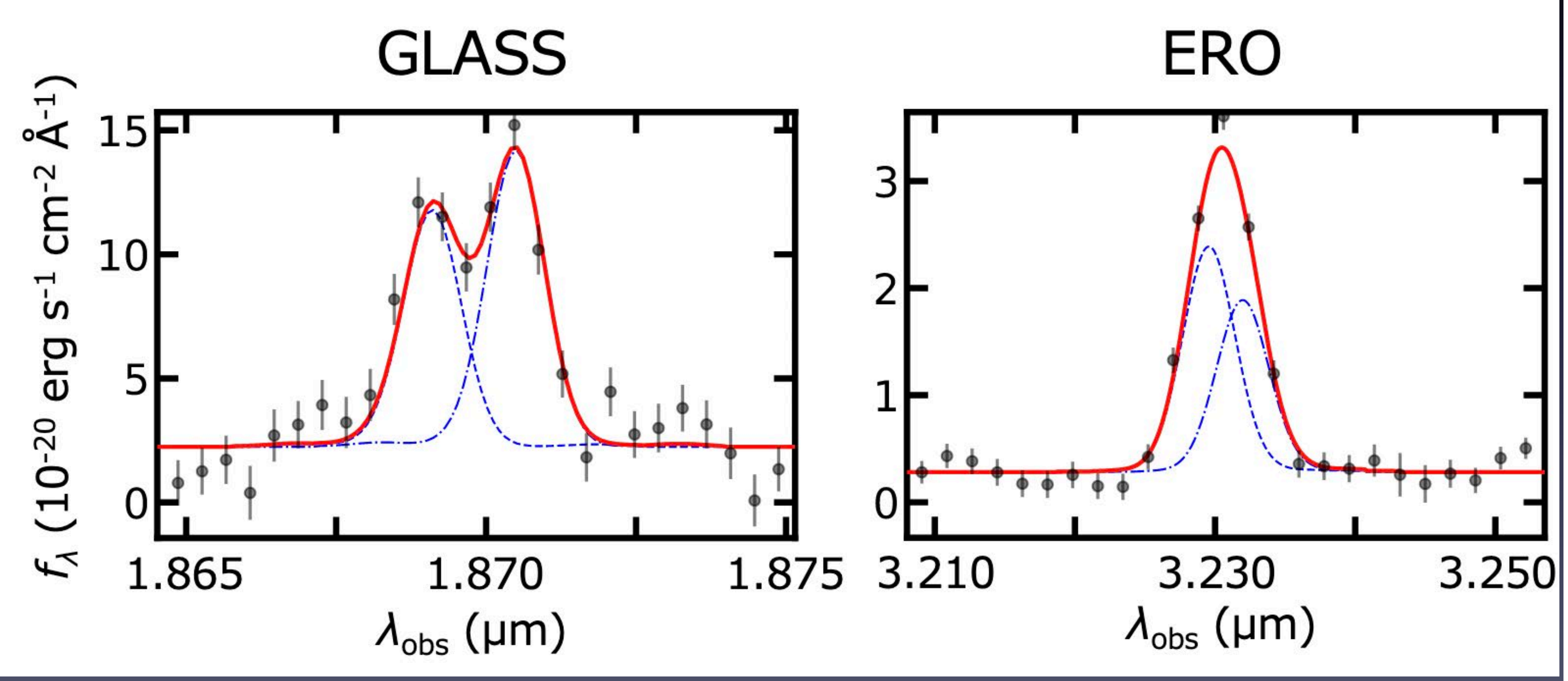

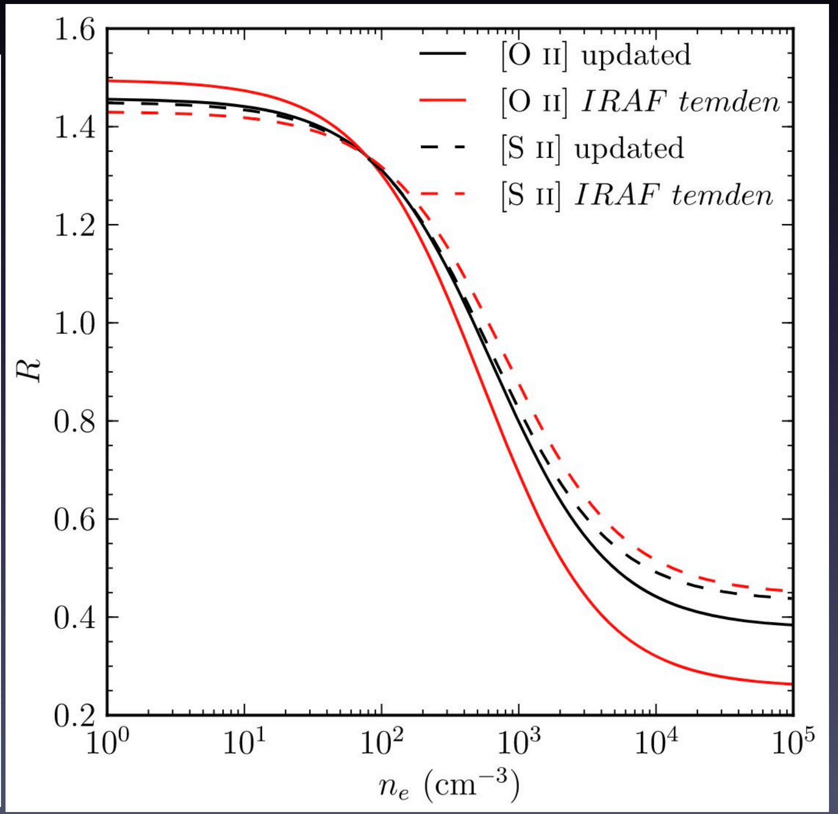

ISM density measurements from NIRSpec Spectroscopy

- GLASS-JWST acquires 17.7k sec in all three high-res gratings (12 exp per grating)
- data reduced using the msaexp software with optimal extraction

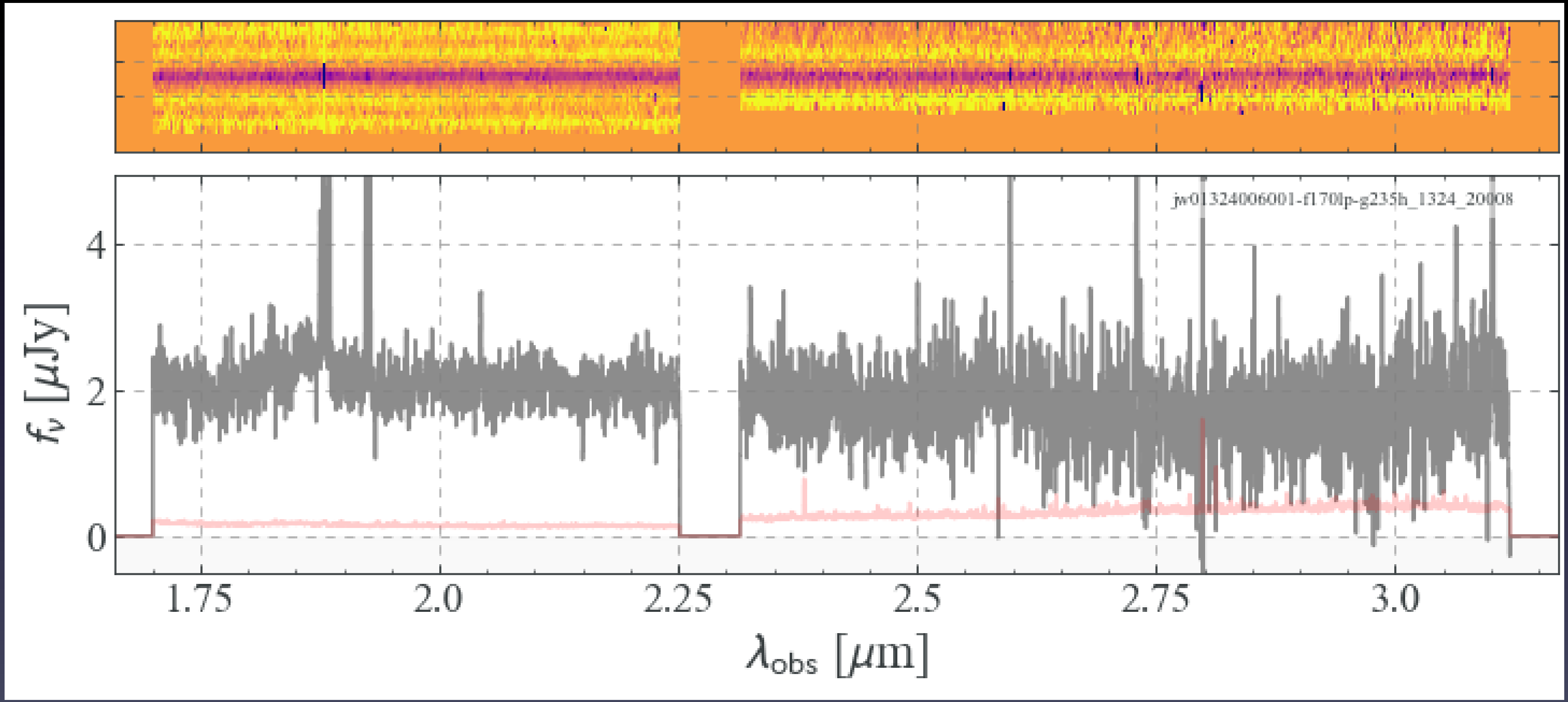

a z~1.86 galaxy with $M_* \sim 2e8\ M_\odot$

Li Sijia, **XW** et al. in prep

ISM electron density measurements from NIRSpec Spectroscopy

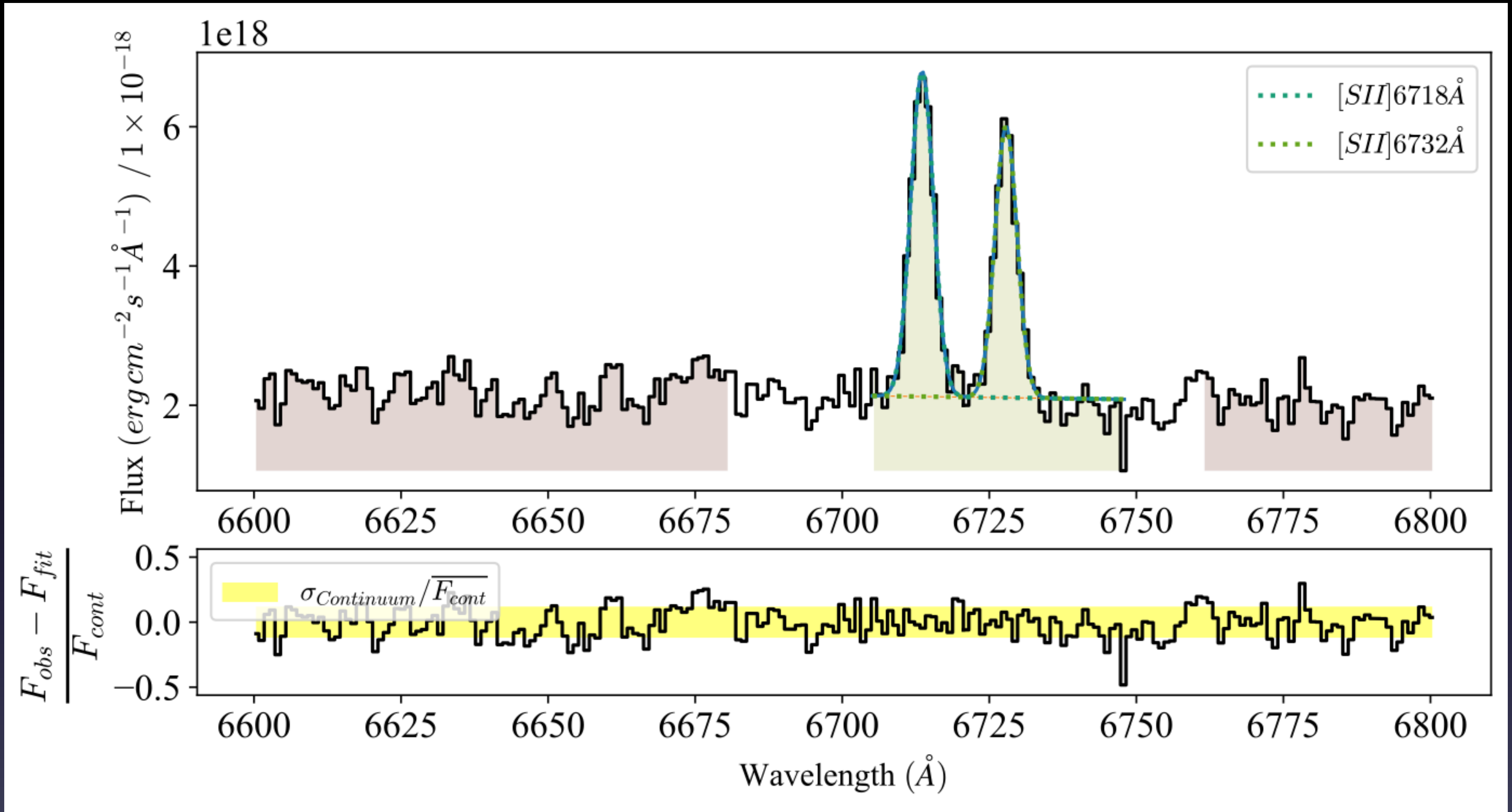

Line	$F_{err,\,gauss}$	$\frac{S}{N}_{line}$	z_{line}	Eqw	Eqw_{err}	F_{gauss}	$\sigma_{i,\,err}$
$[SII]6718\mathring{A}$	0.7863	26.1578	-6.5735e-04	10.6536	0.3699	22.6424	0.0775
$[SII]6732\mathring{A}$	0.7732	21.4849	-6.1716e-04	8.6046	0.3638	18.2876	0.0912

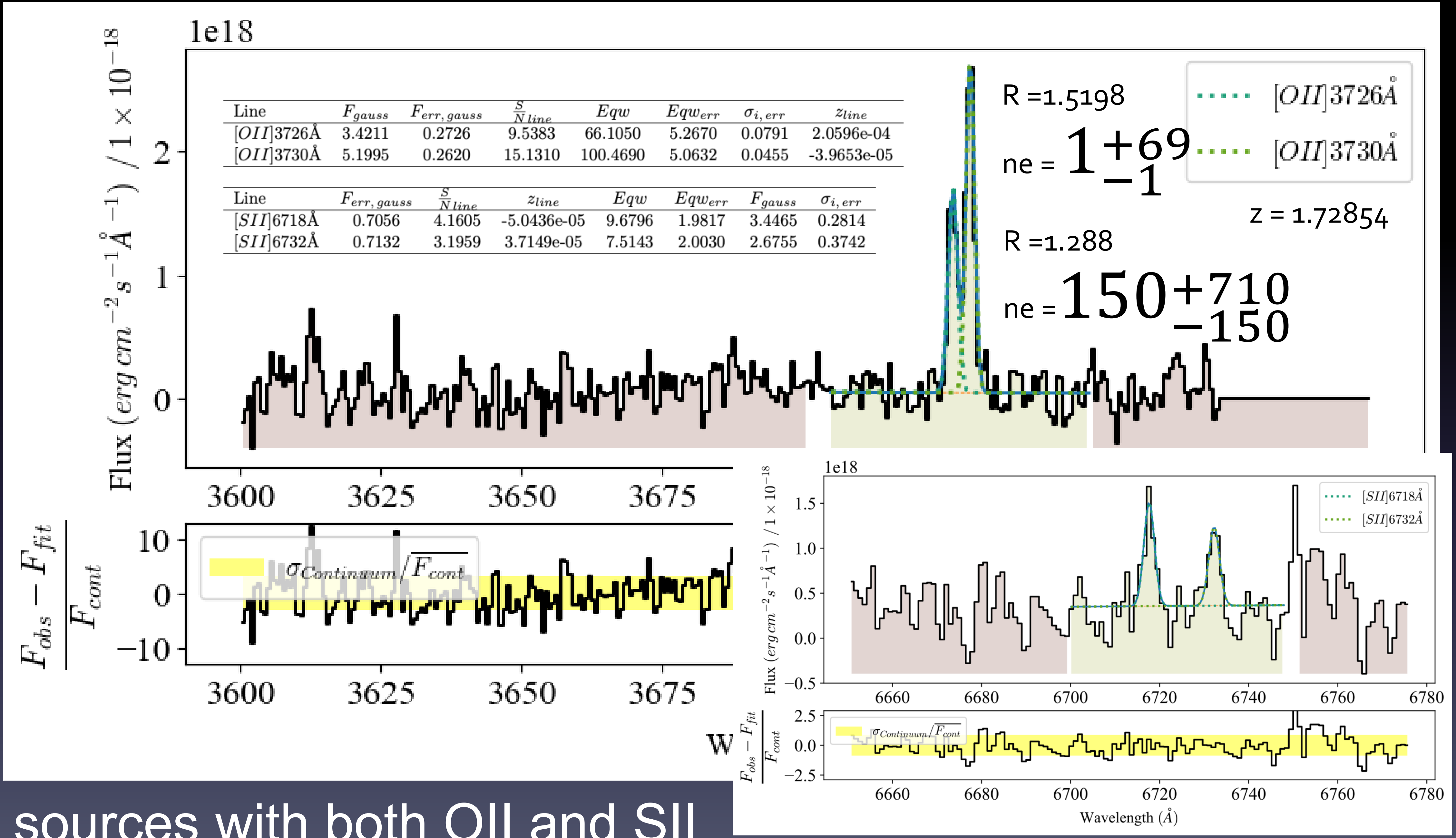

Line	F_{gauss}	$F_{err,\,gauss}$	$\frac{S}{N}_{line}$	Eqw	Eqw_{err}	$\sigma_{i,\,err}$	z_{line}
$[OII]3726\AA$	3.4211	0.2726	9.5383	66.1050	5.2670	0.0791	2.0596e-04
$[OII]3730\AA$	5.1995	0.2620	15.1310	100.4690	5.0632	0.0455	-3.9653e-05

Line	$F_{err,\,gauss}$	$\frac{S}{N}_{line}$	z_{line}	Eqw	Eqw_{err}	F_{gauss}	$\sigma_{i,\,err}$
$[SII]6718\AA$	0.7056	4.1605	-5.0436e-05	9.6796	1.9817	3.4465	0.2814
$[SII]6732\AA$	0.7132	3.1959	3.7149e-05	7.5143	2.0030	2.6755	0.3742

sources with both OII and SII

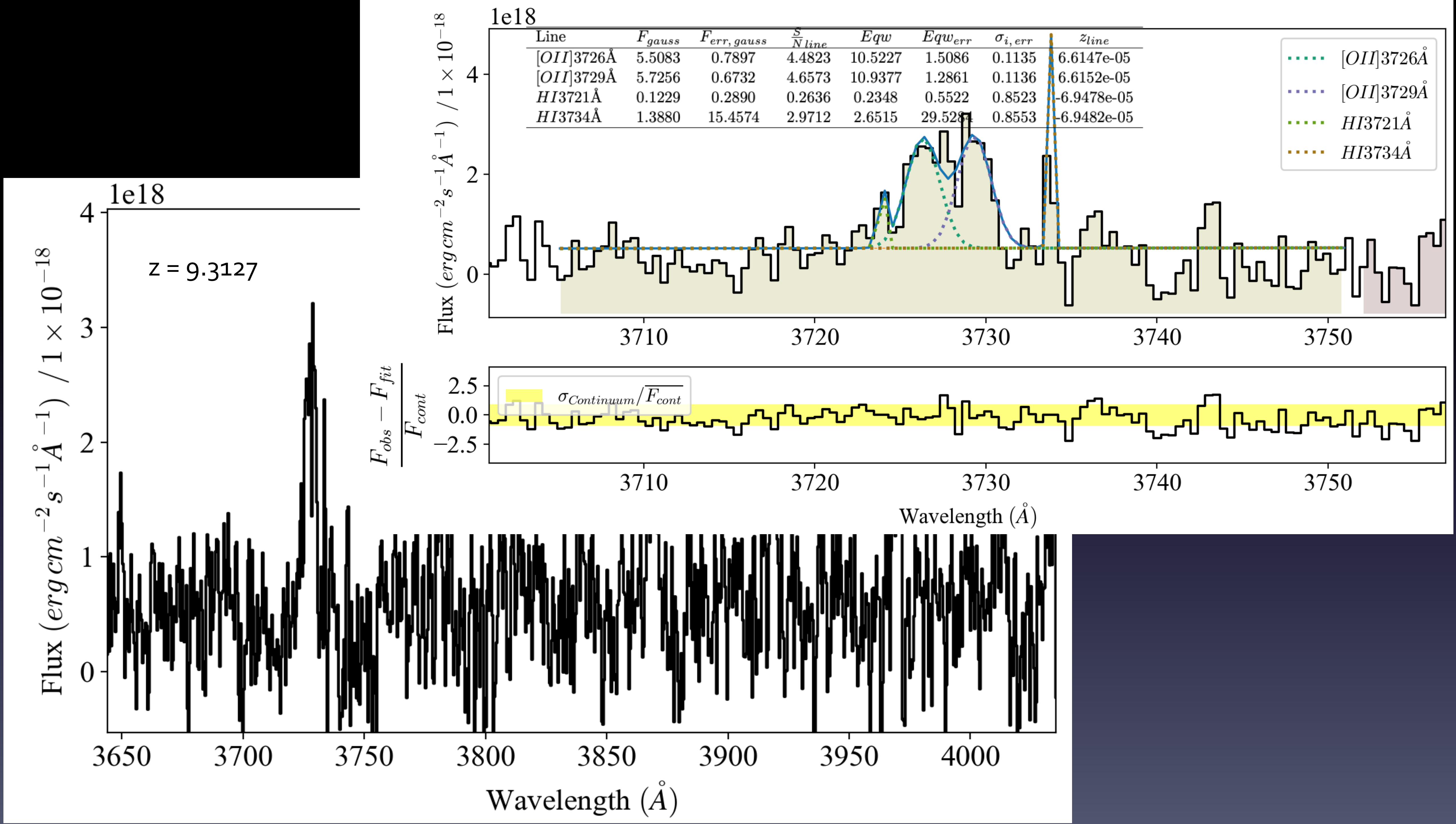

Line	F_{gauss}	$F_{err,\,gauss}$	$\frac{S}{N}_{line}$	Eqw	Eqw_{err}	$\sigma_{i,\,err}$	z_{line}
$[OII]3726\mathring{A}$	5.5083	0.7897	4.4823	10.5227	1.5086	0.1135	6.6147e-05
$[OII]3729\mathring{A}$	5.7256	0.6732	4.6573	10.9377	1.2861	0.1136	6.6152e-05
$HI3721\mathring{A}$	0.1229	0.2890	0.2636	0.2348	0.5522	0.8523	-6.9478e-05
$HI3734\mathring{A}$	1.3880	15.4574	2.9712	2.6515	29.5284	0.8553	-6.9482e-05

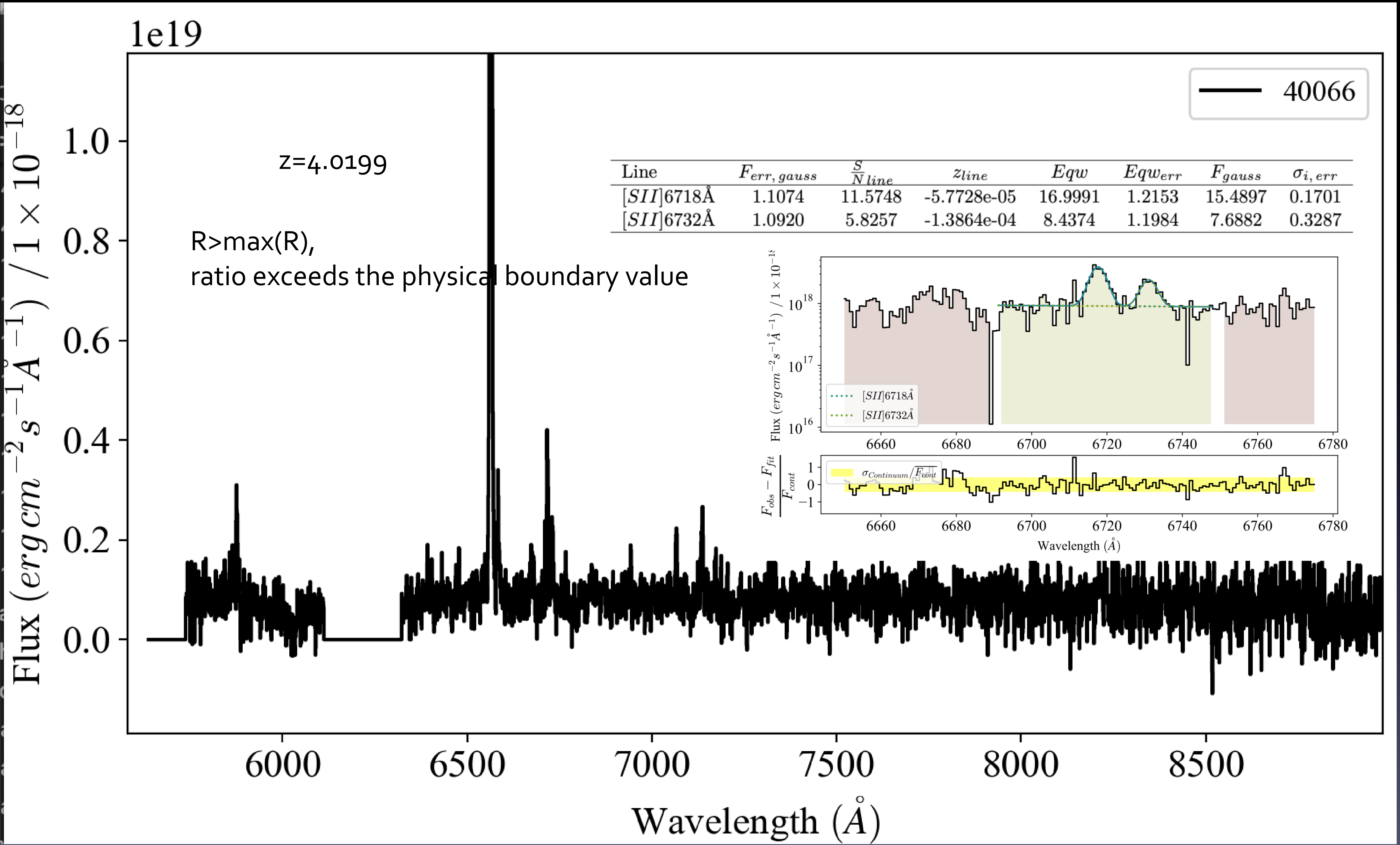

z=4.0199

R>max(R),
ratio exceeds the physical boundary value

Line	$F_{err,\,gauss}$	$\frac{S}{N}_{line}$	z_{line}	Eqw	Eqw_{err}	F_{gauss}	$\sigma_{i,\,err}$
$[SII]$6718Å	1.1074	11.5748	-5.7728e-05	16.9991	1.2153	15.4897	0.1701
$[SII]$6732Å	1.0920	5.8257	-1.3864e-04	8.4374	1.1984	7.6882	0.3287

Evolution of ISM density with sSFR and z

Li Sijia, **XW** et al. in prep

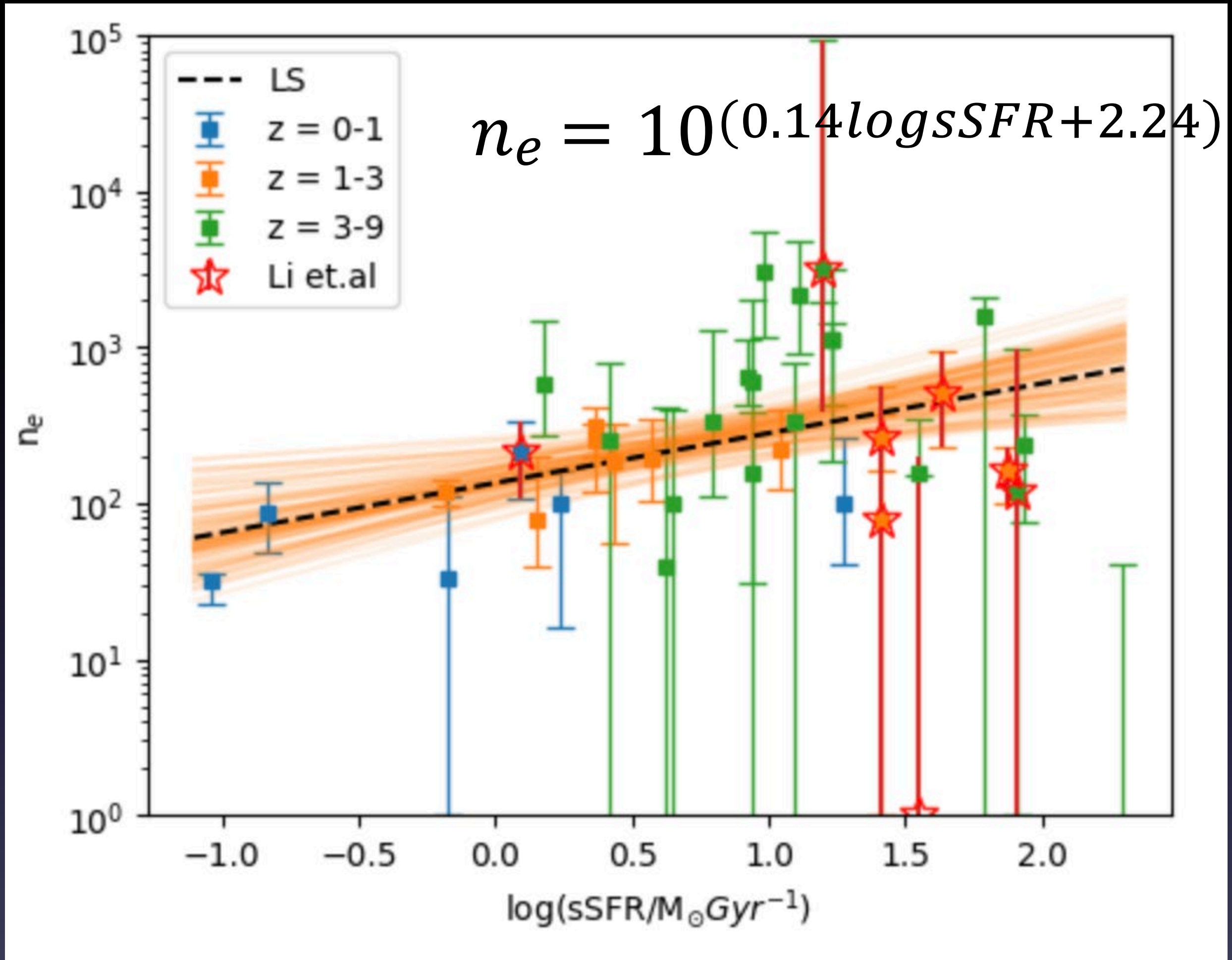

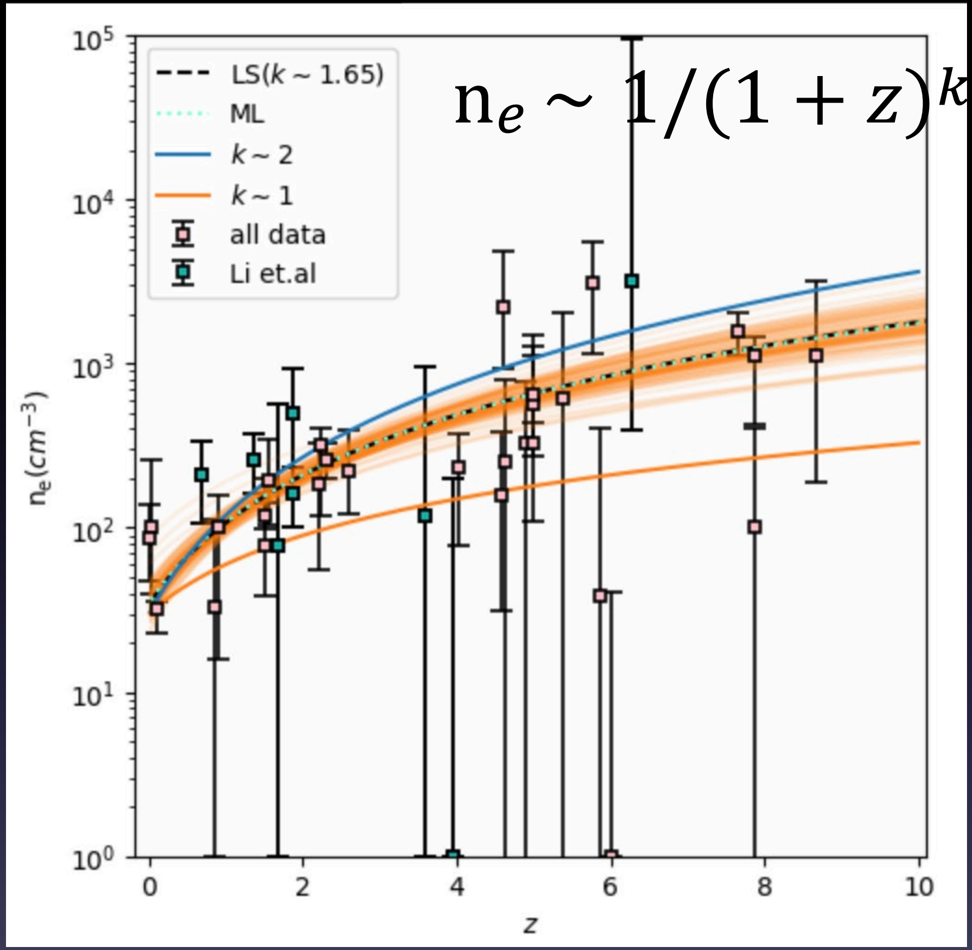

- positive correlation between n_e and sSFR => dense ISM conducive to star formation
- redshift evolution of n_e consistent with galaxy size evolution

A He II λ1640 emitter with blue UV spectral slope at z=8.16

Wang et al. 2022b

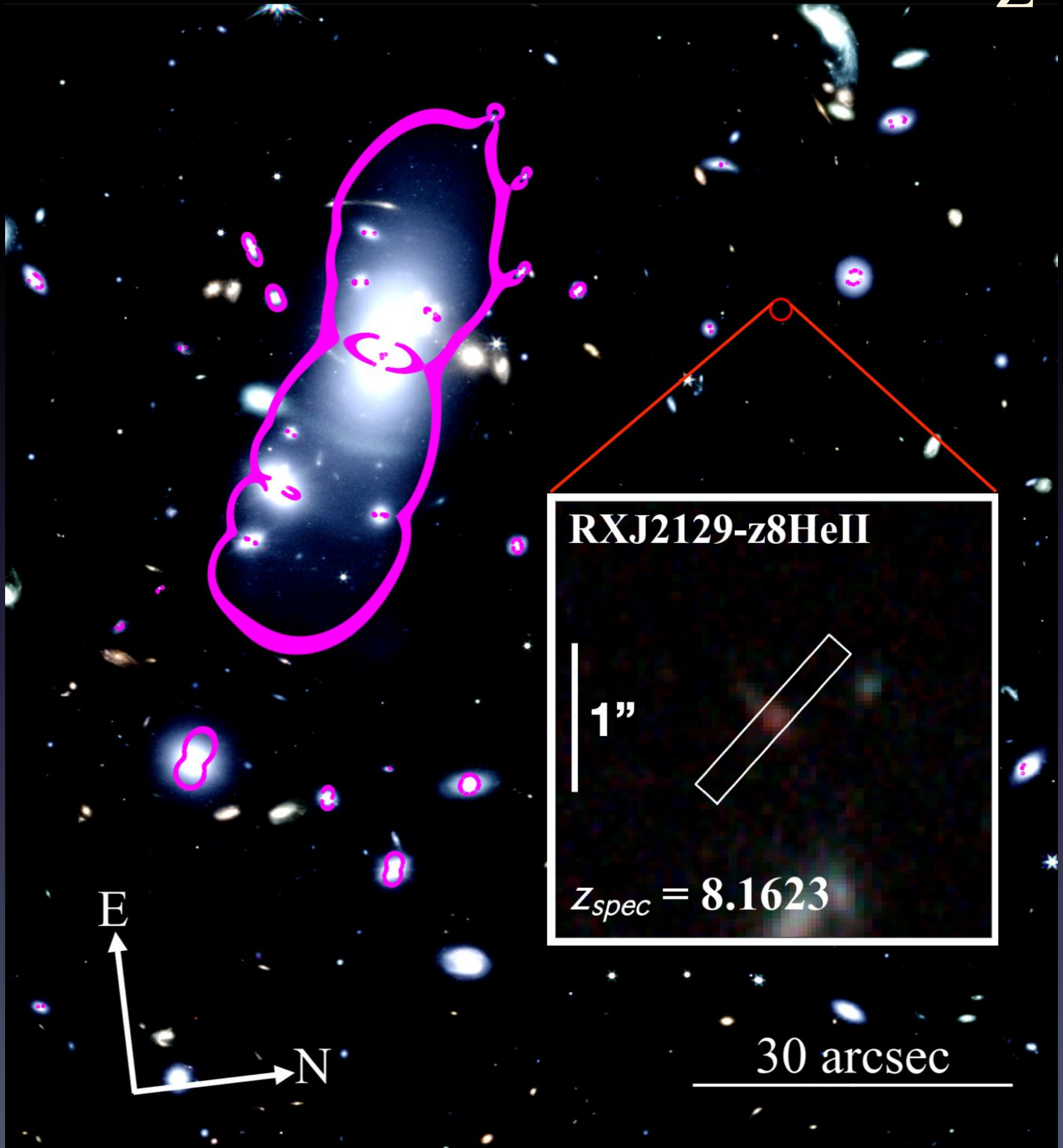

- a strong emission-line galaxy at z=8.16
- lensed by the foreground galaxy cluster RXJ2129.7+0005 at z=0.234
- data acquired by DD-2767 (PI: Kelly)

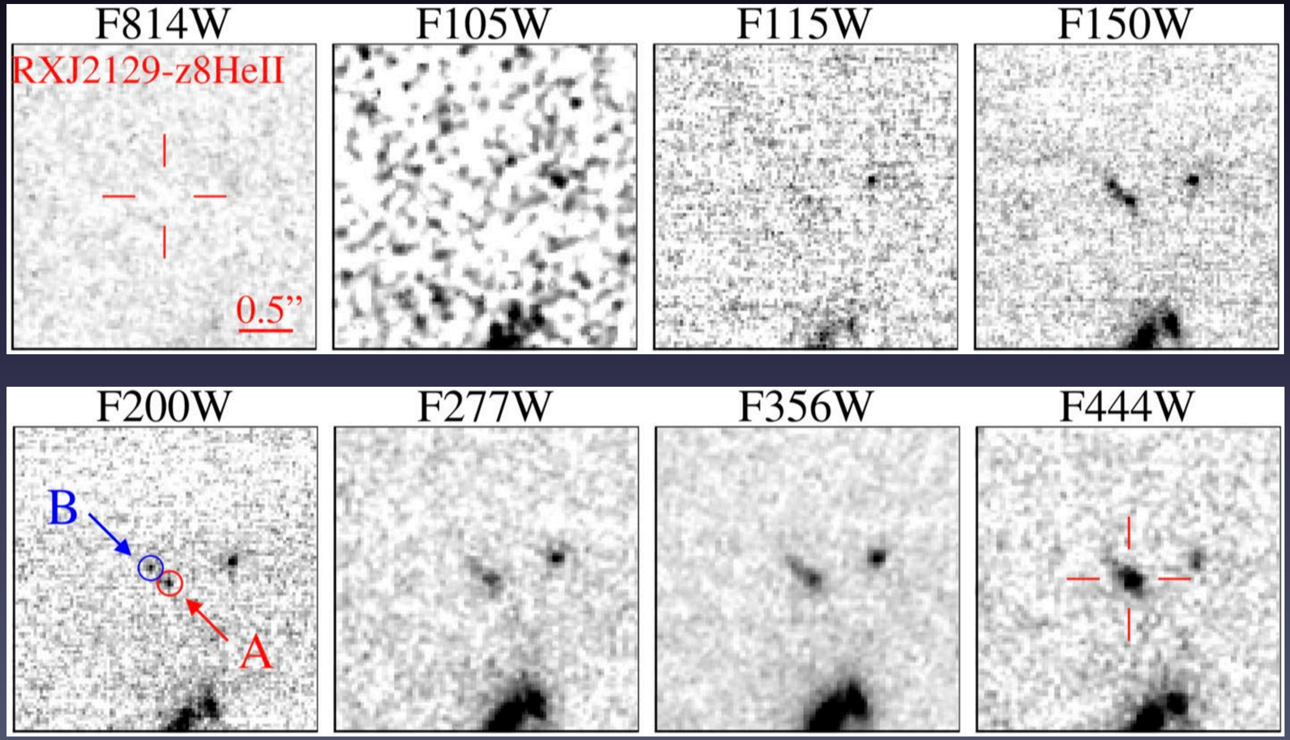

A He II λ1640 emitter with blue UV spectral slope at z=8.16

Wang et al. 2022b

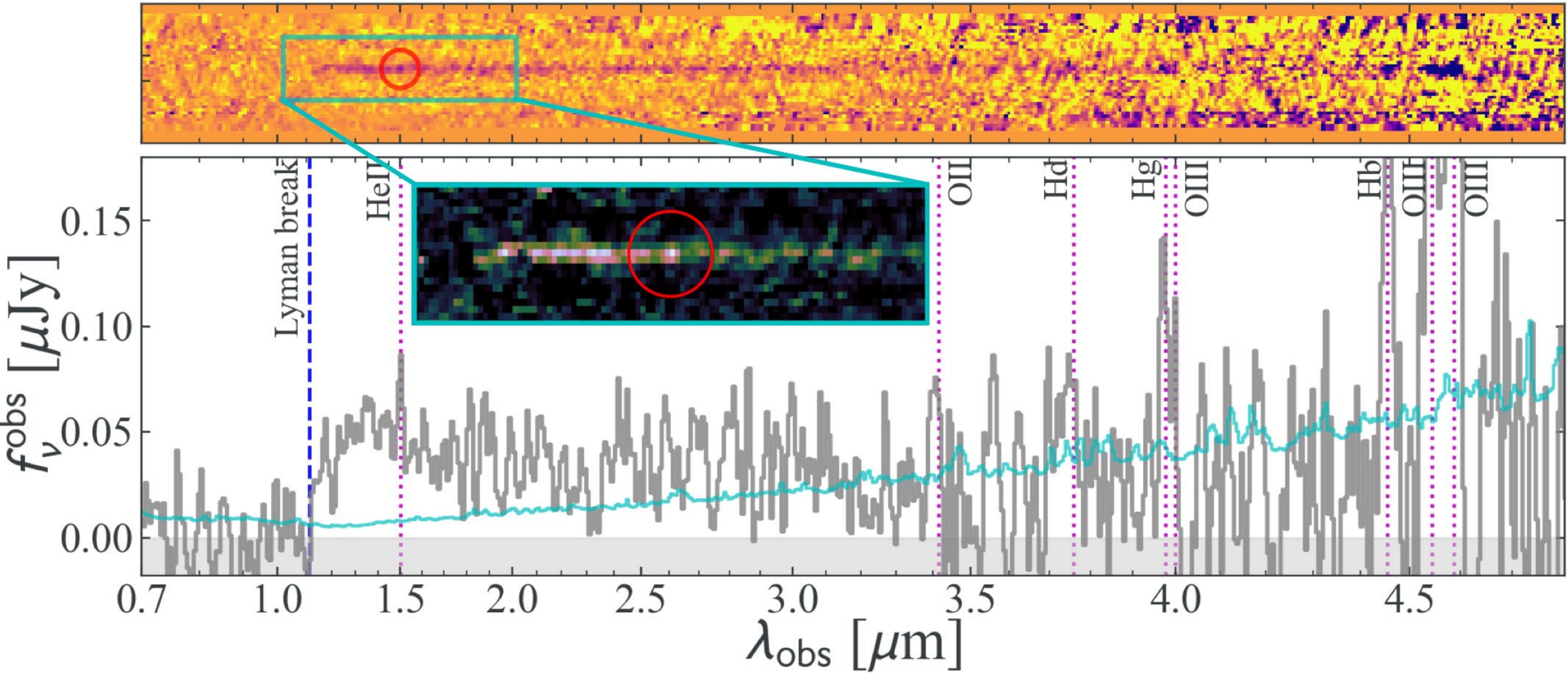

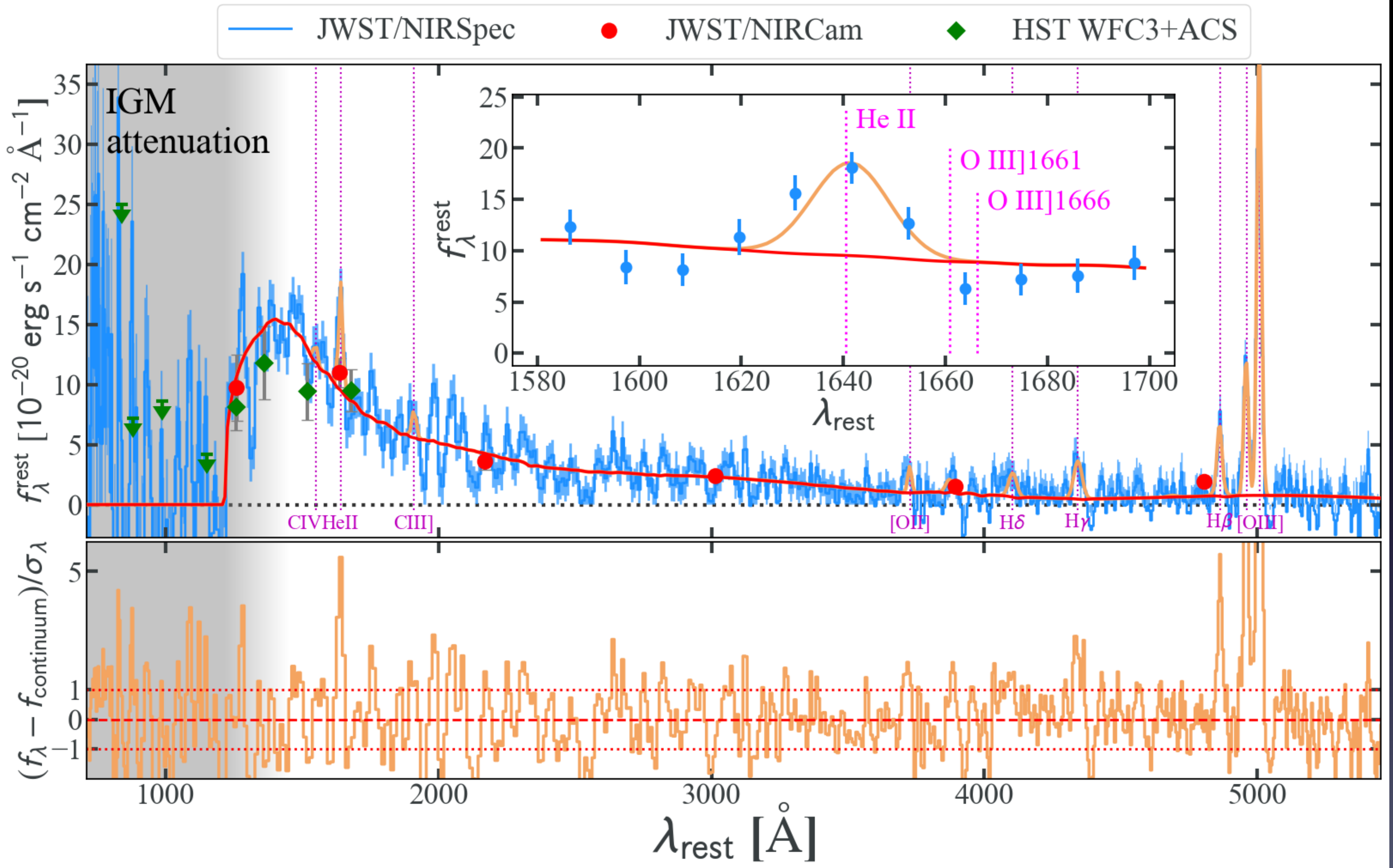

JWST/NIRSpec
JWST/NIRCam
HST WFC3+ACS
IGM attenuation
He II
O III]1661
O III]1666
CIV
HeII
CIII]
[OII]
Hδ
Hγ
Hβ
[OIII]
λrest
λrest [Å]

Extremely blue UV spectral slope

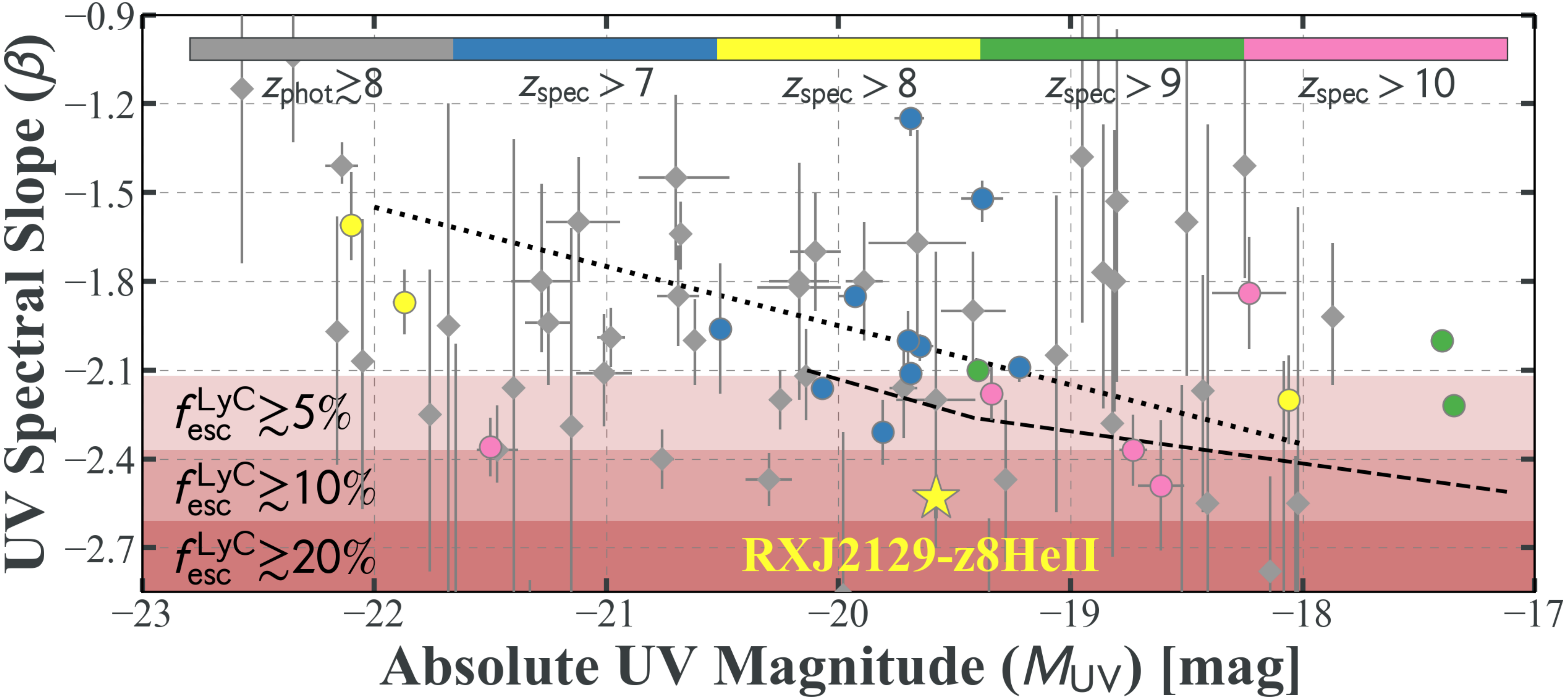

RXJ2129-z8HeII is one of a kind!

1. It shows a strong He II λ1640 line emission, with one of the largest equivalent widths (~21 Å in the rest frame) and high flux ratios versus metal/hydrogen lines.
2. It has one of the steepest continuum slope of rest-frame UV spectrum among galaxies spectroscopically confirmed in the epoch of reionization.
3. It belongs to the intrinsically faint galaxy population (below the characteristic luminosity), has high flux ratio of the triply and doubly ionized oxygen lines ([O III]/[O II]) in the rest-frame optical with high equivalent width.

Strong He II λ1640 line

- One of the highest redshift He II detection in the literature:
  - line flux (corr. for magnif and dust): 120±22 $\times 10^{-20}$ erg $s^{-1} cm^{-2}$
  - equivalent width: 21±4 Å
- Possible causes for strong He II emission:
  - Wolf-Rayet stars, stripped stars
  - X-ray binaries
  - active galactic nuclei
  - **Pop III stars** (high-mass, metal-free, first generation stars)

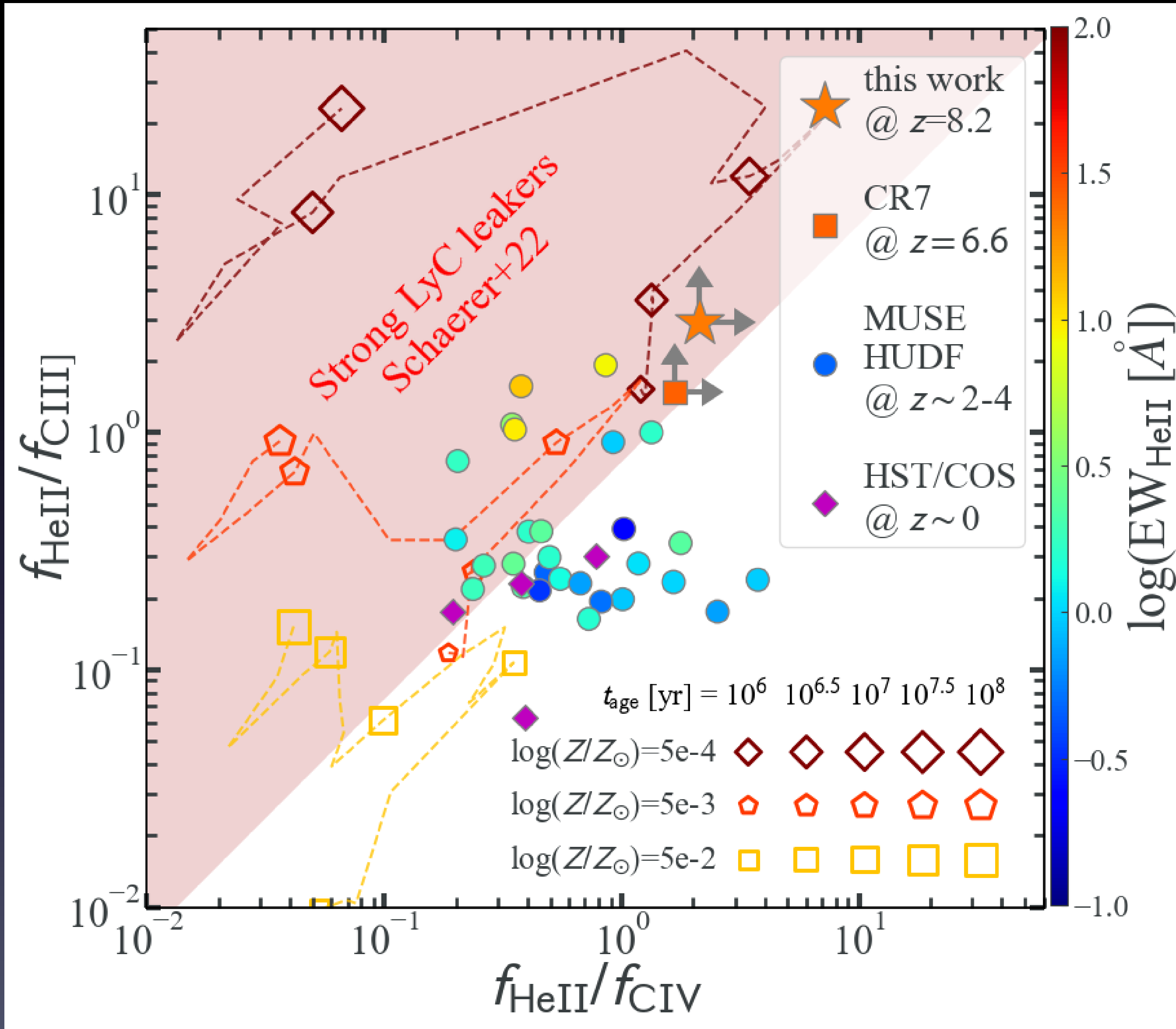

Photoionization models for Pop III stars

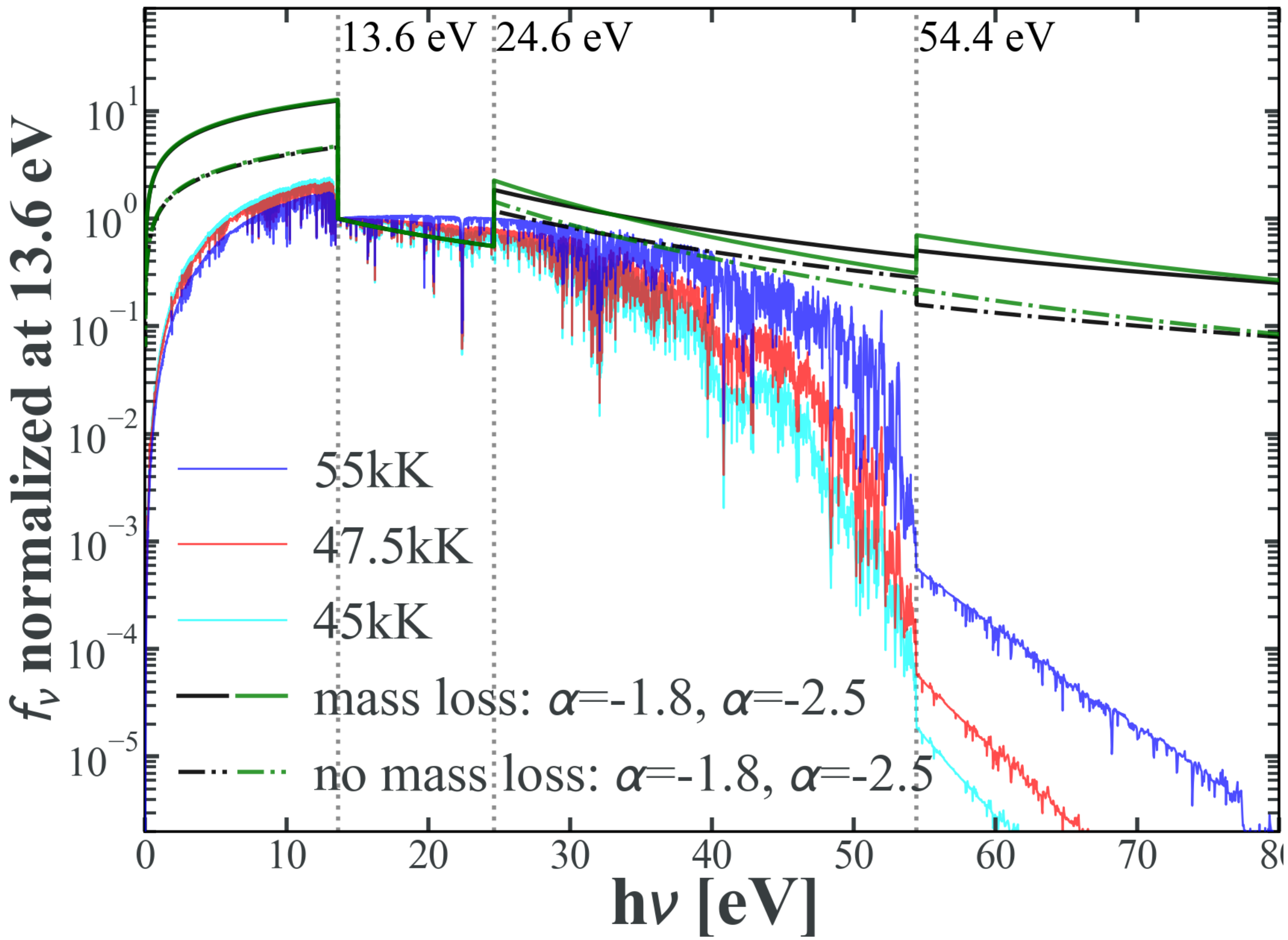

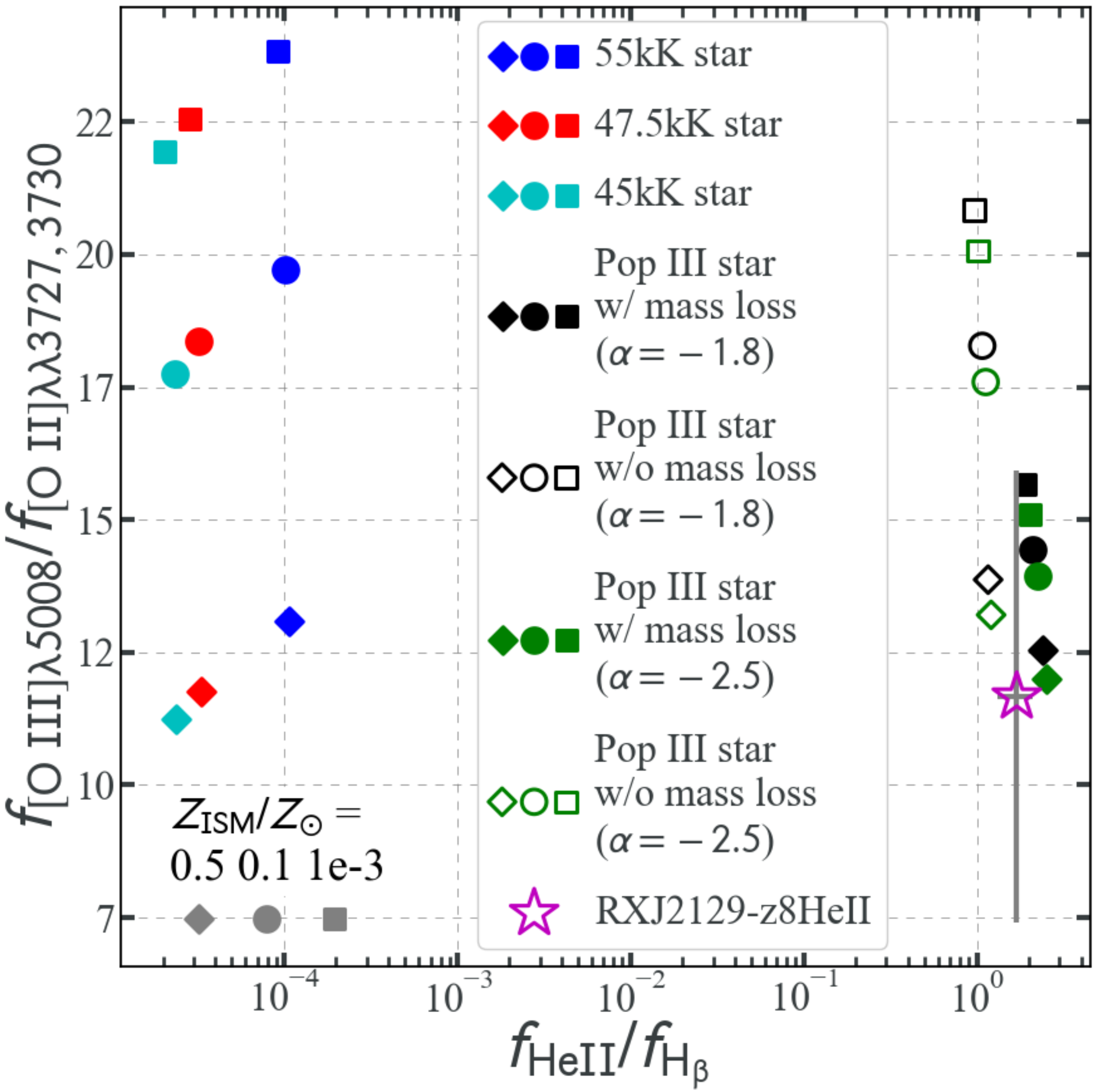

O32 alone not a good proxy of Pop III !!!

Clumpy morphology

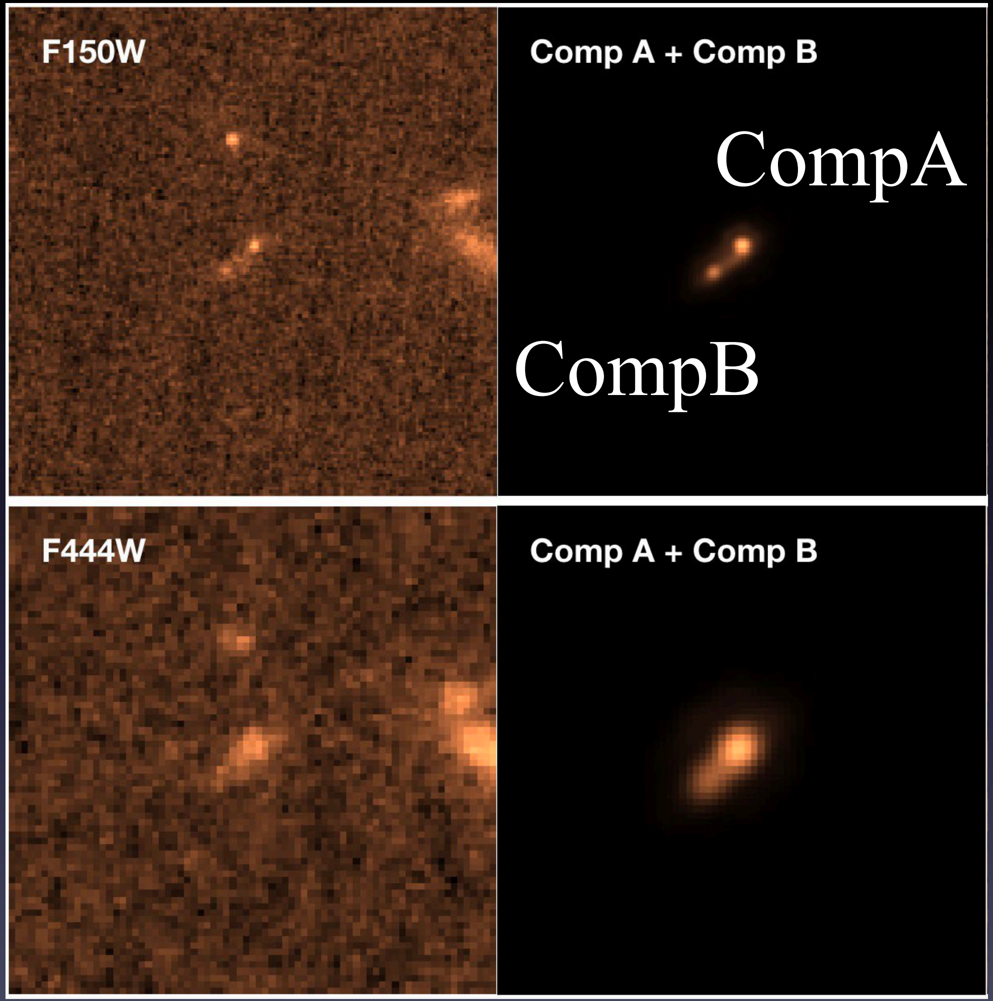

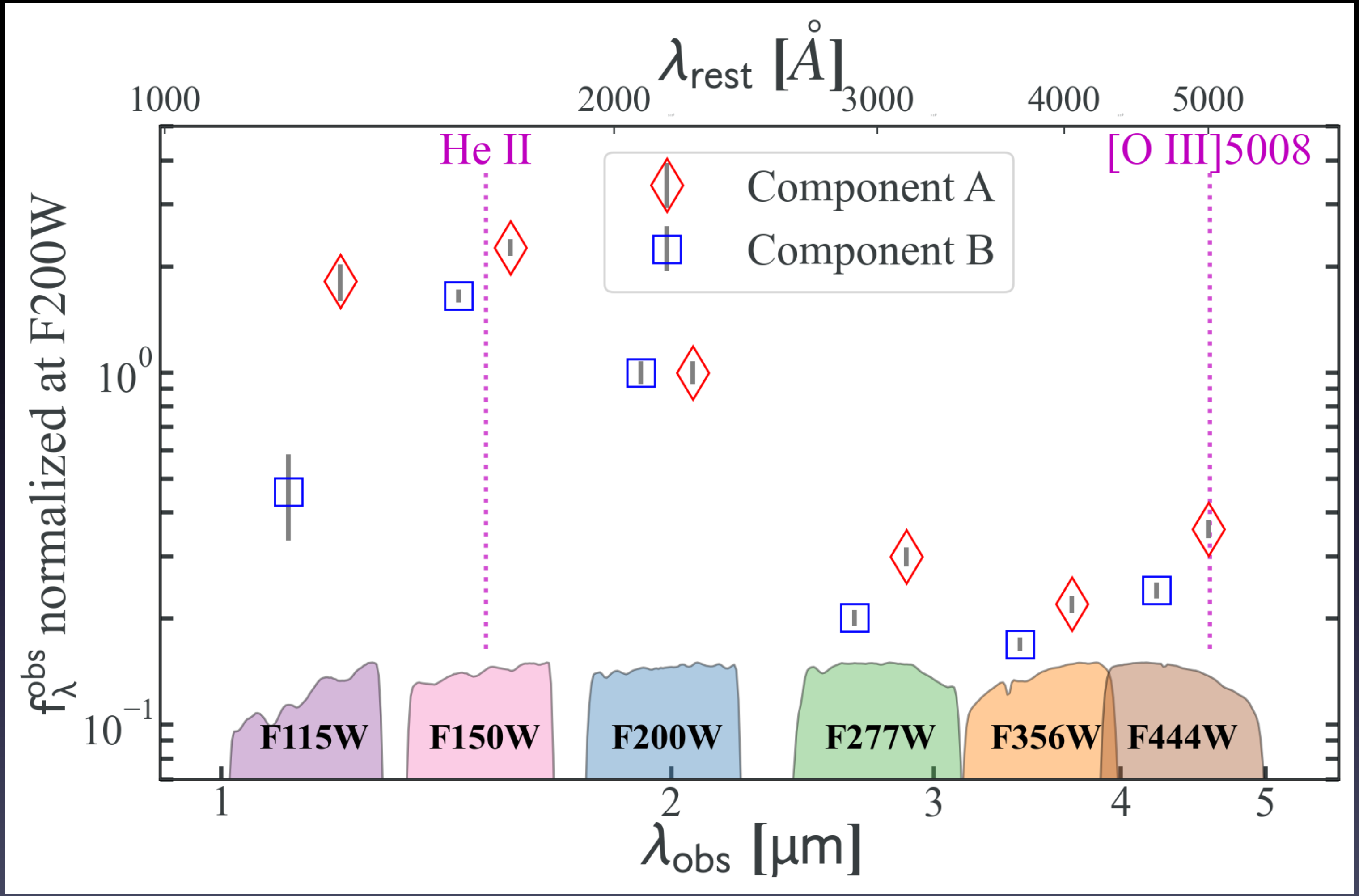

PopIII star formation rate and total mass

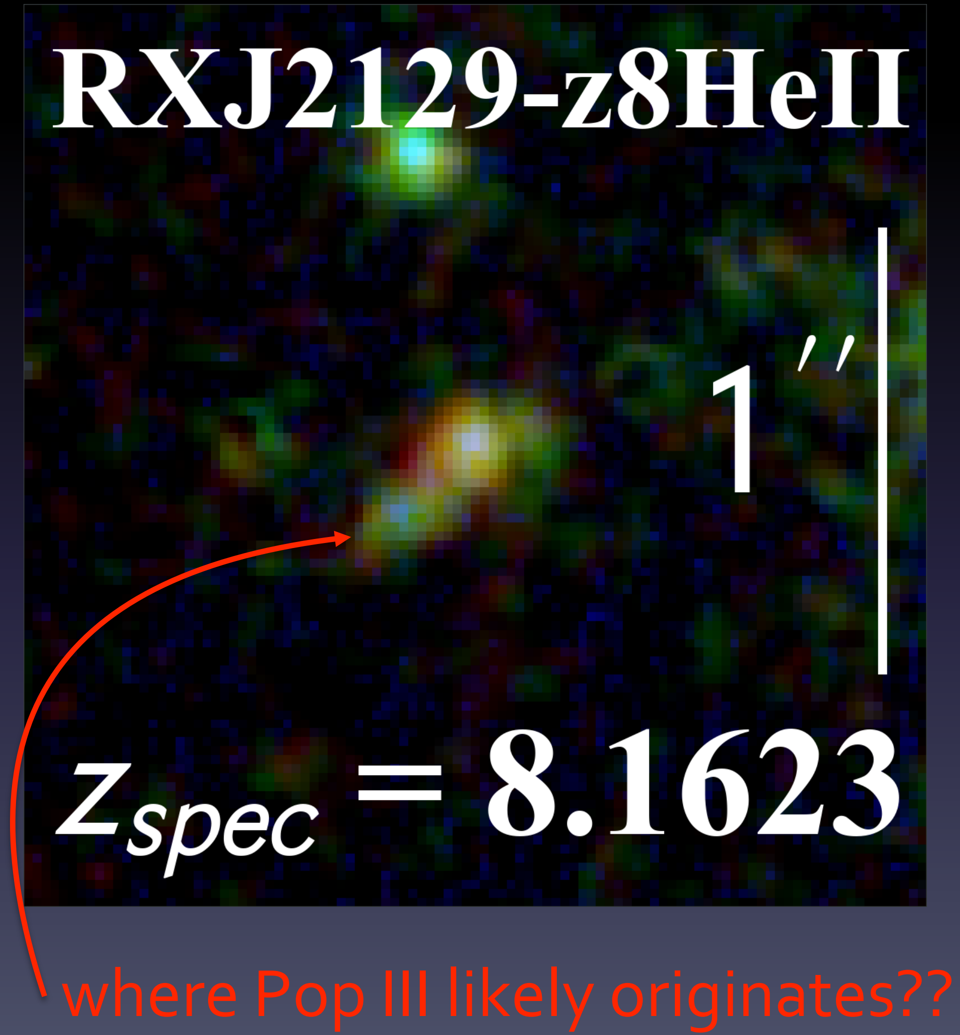

IMF mass range	Mass Loss	$L_{\rm norm,1640}$ [ergs s^{-1}]	$SFR_{\rm PopIII}$ [$M_\odot$ yr^{-1}]	$f_{\rm PopIII}$
$1 \lesssim M/M_\odot \lesssim 500$	No	5.7×10^{40}	5.9	62%
$50 \lesssim M/M_\odot \lesssim 500$	No	3.5×10^{41}	1.0	10%
$1 \lesssim M/M_\odot \lesssim 500$	Yes	1.8×10^{41}	1.8	19%
$50 \lesssim M/M_\odot \lesssim 1000$	Yes	1.4×10^{42}	0.2	2%

- based on the PopIII stellar evolution models of Schaerer 2002
- observed line ratios well reproduced by the Pop III models with mass loss and one tenth ISM metallicity
- total mass: $7.8 \pm 1.4 \times 10^5 M_\odot$ assuming Eddington limit

Conclusions

- Part I: Metallicity radial gradients from NIRISS WFSS.
  - secure first metal gradient measurement at $z \geq 3$ with JWST
  - inverted gradient caused by low-Z gas inflow from tidal interactions
  - JWST's exquisite resolution and sensitivity resolve $z \sim 3$ dwarf in ≥50 elements
- Part II: ISM electron densities from NIRSpec high-resolution spectroscopy.
  - obtain n_e for 10 galaxies based on [SII] flux ratios
  - find positive correlation between n_e and sSFR
  - sharper redshift evolution of n_e derived from [SII] than that from [OII]
- Part III: An intriguing He II λ1640 emitter at $z=8.16$.
  - one of the highest He II detections in the literature
  - one of the steepest UV slopes among spec. confirmed galaxies at $z \geq 7$
  - enticing implication for the coexistence of PopIII and normal stars

Thanks for your attention!

Backup slides

Spectral stacking analysis of 1D grism spectra

- Stacking the optimally extracted 1D spectra of multiple sources within the same stellar mass bin to achieve higher SNR
- Measure the correlation at the population level

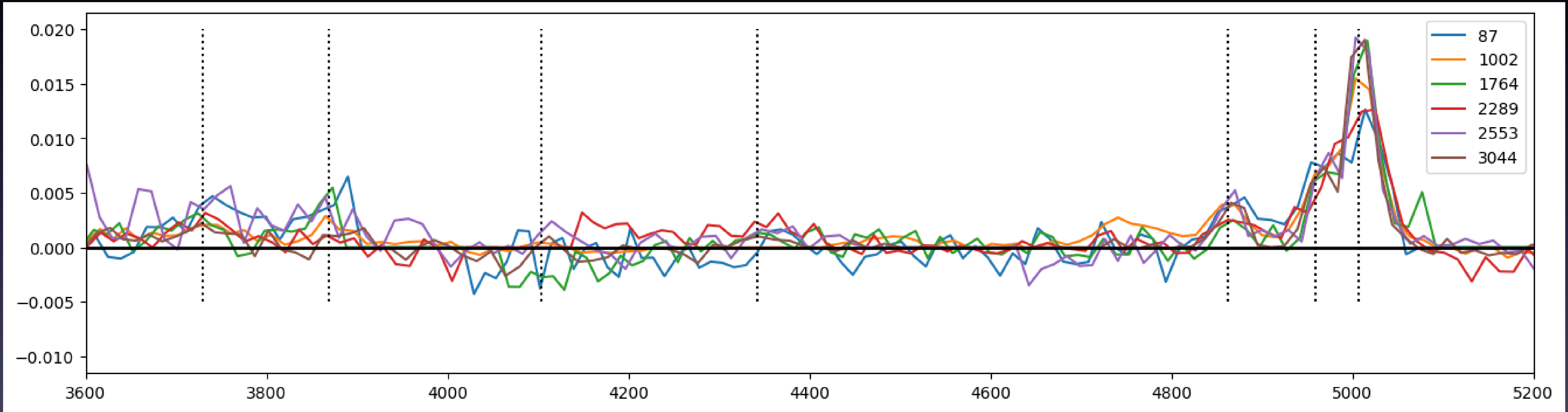

He Xianlong, XW et al. in prep

Line flux of LMfit vs Grizili

Grizli models higher emission line flux

$$\lg(grizli) = \lg(lmfit) + (0.168 \pm 0.021)$$
$$or{:}grizli = lmfit \times (1.473^{+0.072}_{-0.070})$$

- Pearson/Spearman r correlation: 0.889,0.872, with p-value both ~1e-16

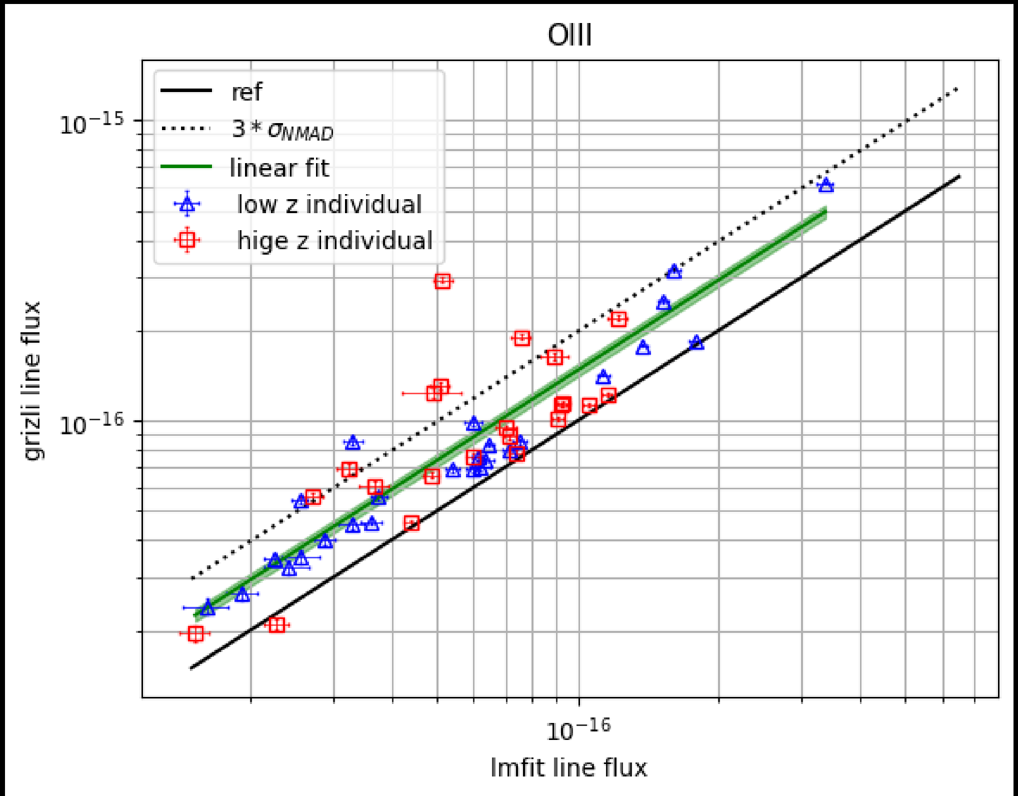

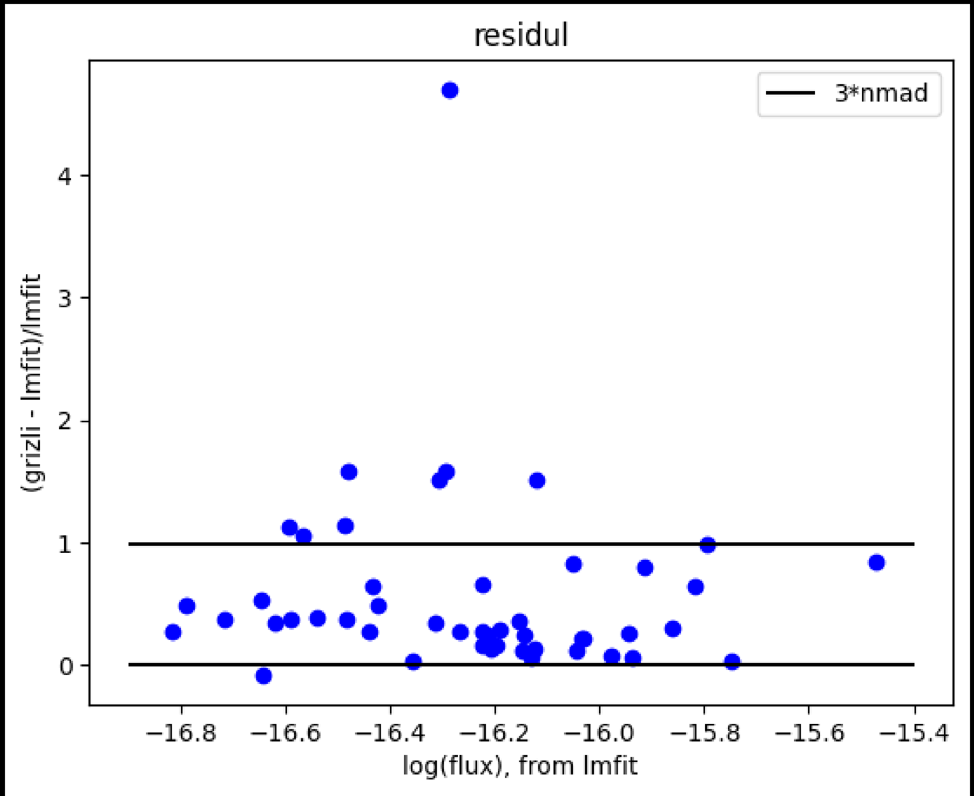

The diverse chemical profiles of high-z galaxies

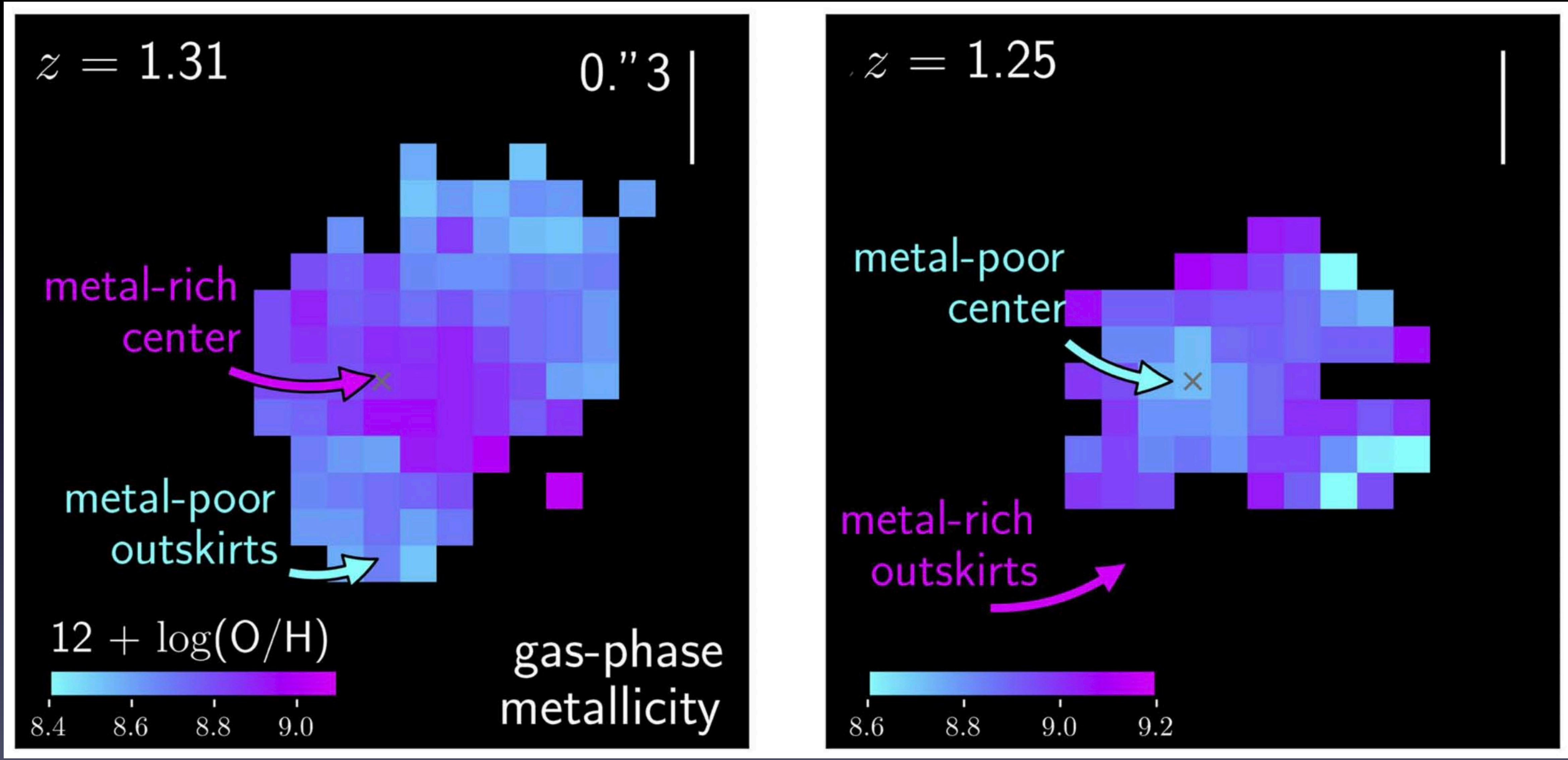

Simons, Papovich, +CLEAR team (2021)

The reason for GLASS-Zgrad1 showing inverted gradients

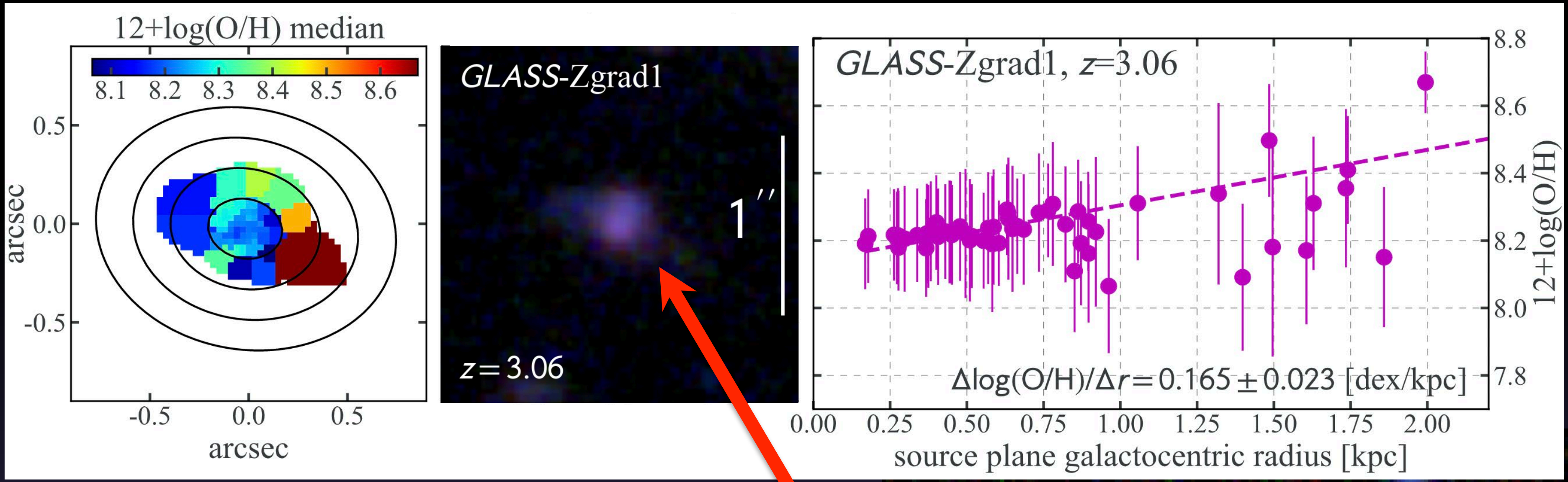

- metal-poor gas inflows to the inner galaxy disks induced by the strong tidal torques of close gravitational interactions

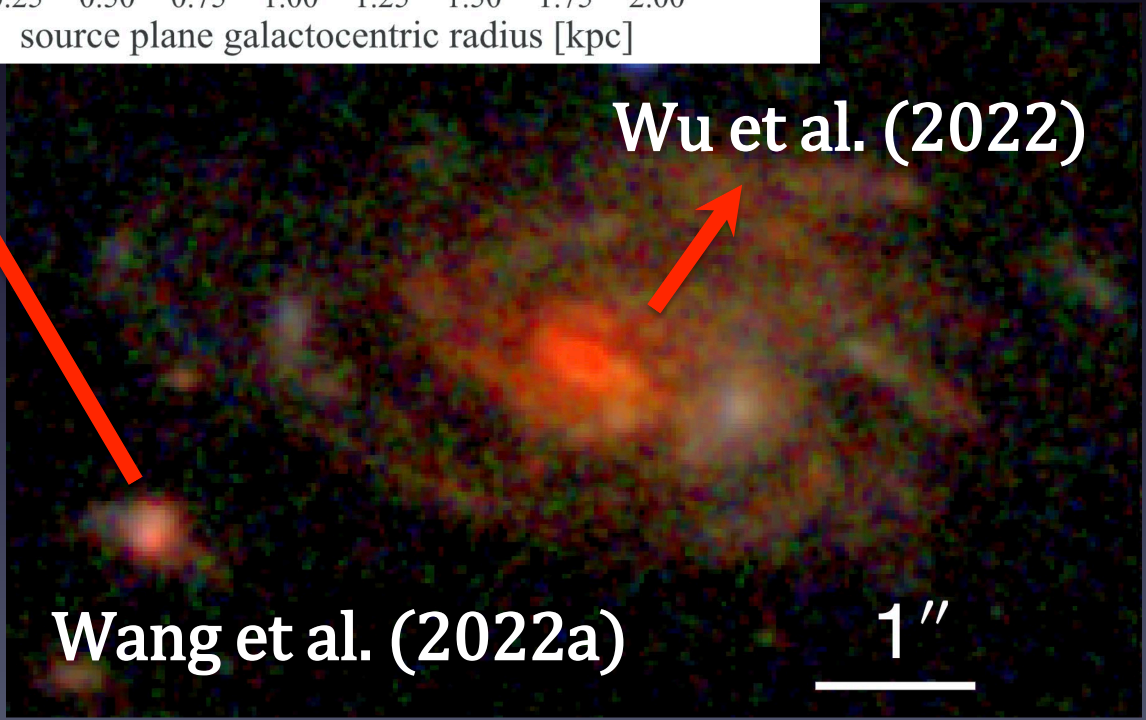

motivation of having both NIRISS and NIRSpec spectra

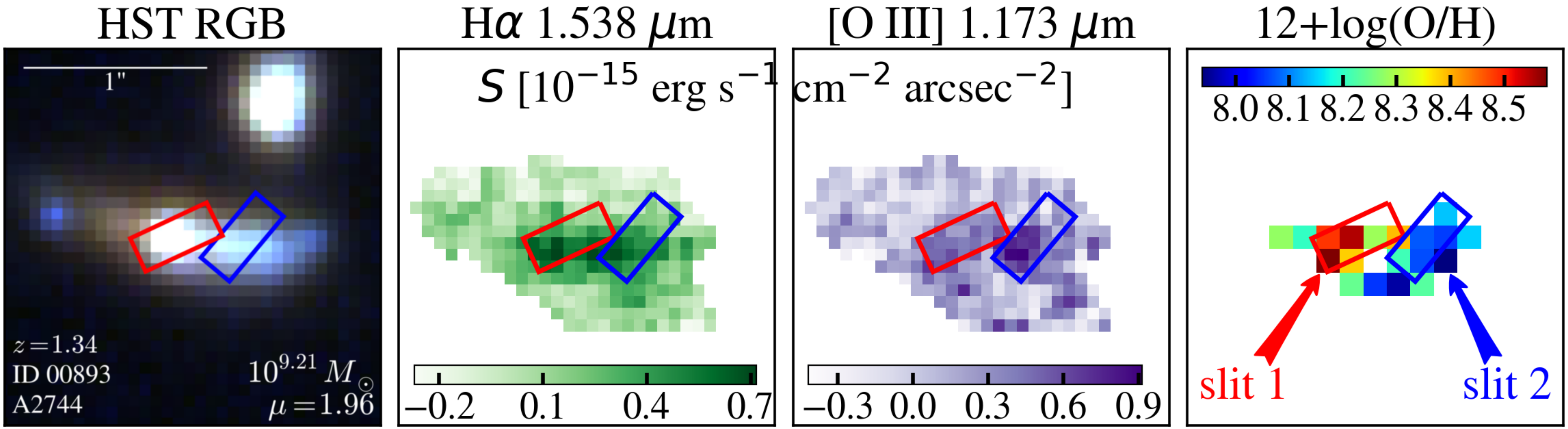

- real data from HST WFC3 grisms (progID 13459, PI: Treu)
- slit size: 0.2”x0.46”, red on bulge, blue on disk
- clear metallicity, dust and SFR gradient from bulge to disk

motivation of having both NIRISS and NIRSpec spectra

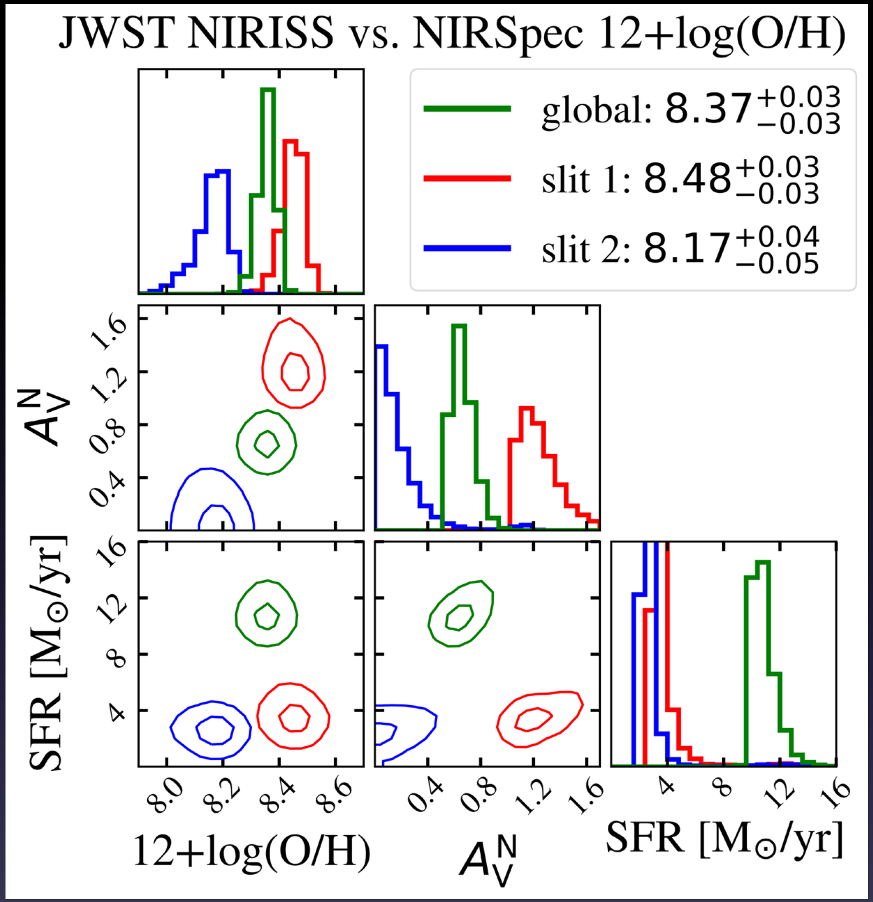

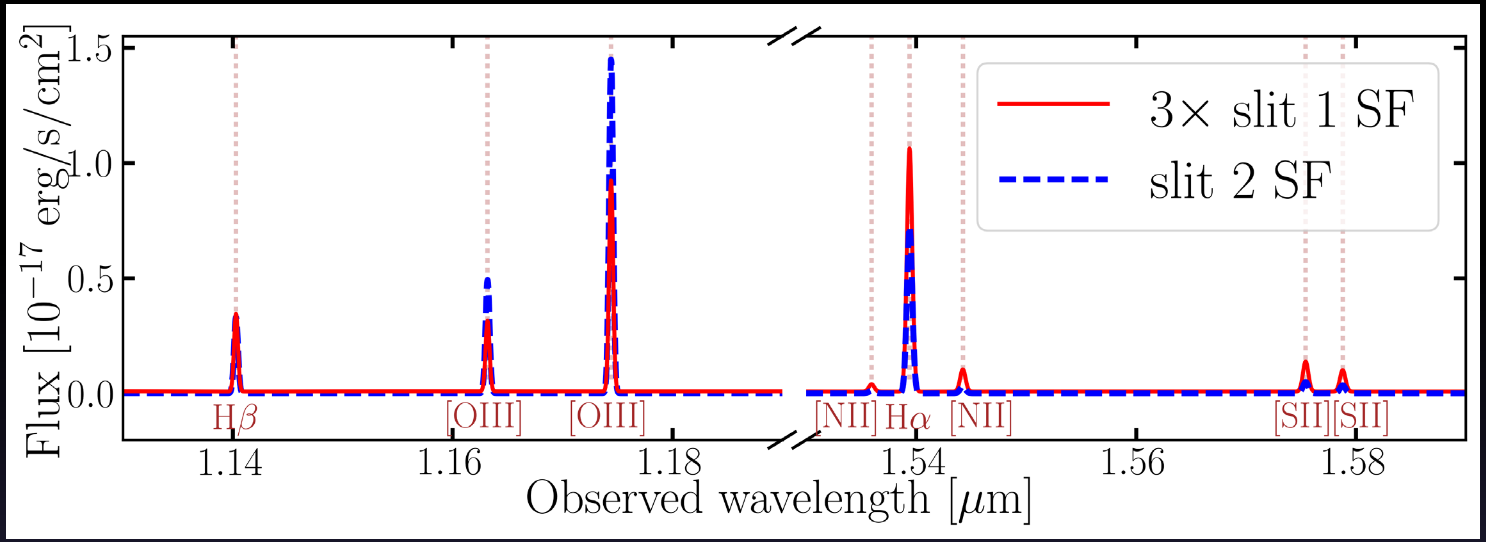

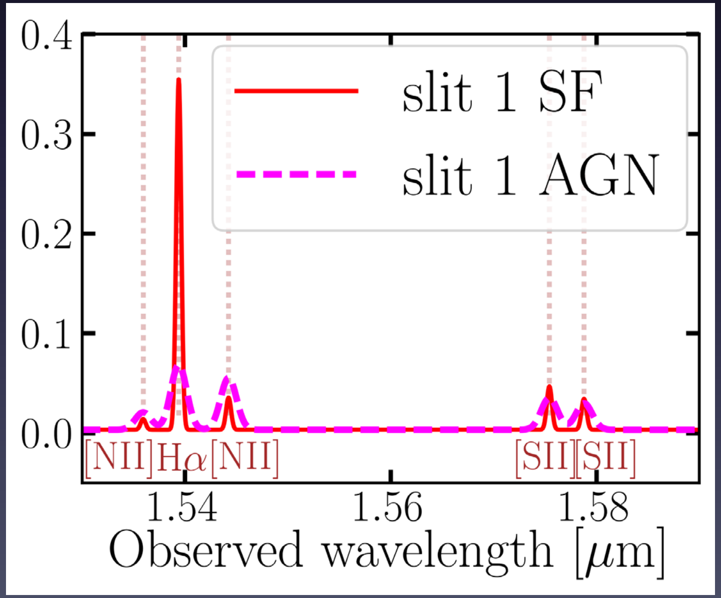

- WFSS cannot distinguish SF/AGN due to spec. reso
- slit spec suffers from slit loss, measurement bias, etc.

combined NIRCam mosaics of A2744

- combing the NIRCam data from multiple programs
- GLASS: green
  - mAB ~ 29-29.4
- UNCOVER: blue
  - mAB ~ 29.8
- Chen DDT: red
  - mAB ~ 29

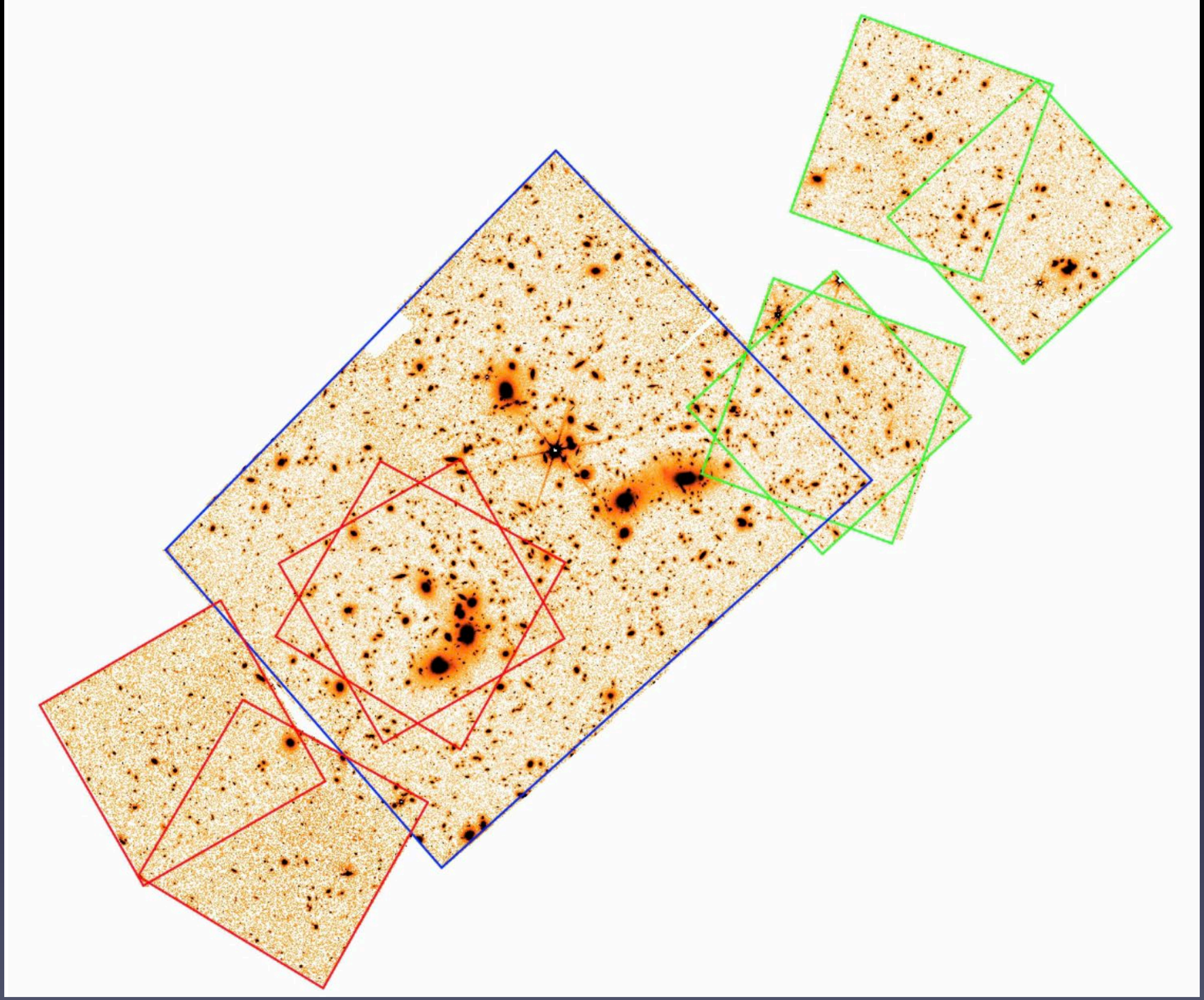

Discovery of strongly inverted metal gradients at high z

- analytical chemical evolution model of galaxy formation assuming inside-out growth predicts initially steep negative gradients flatten over time

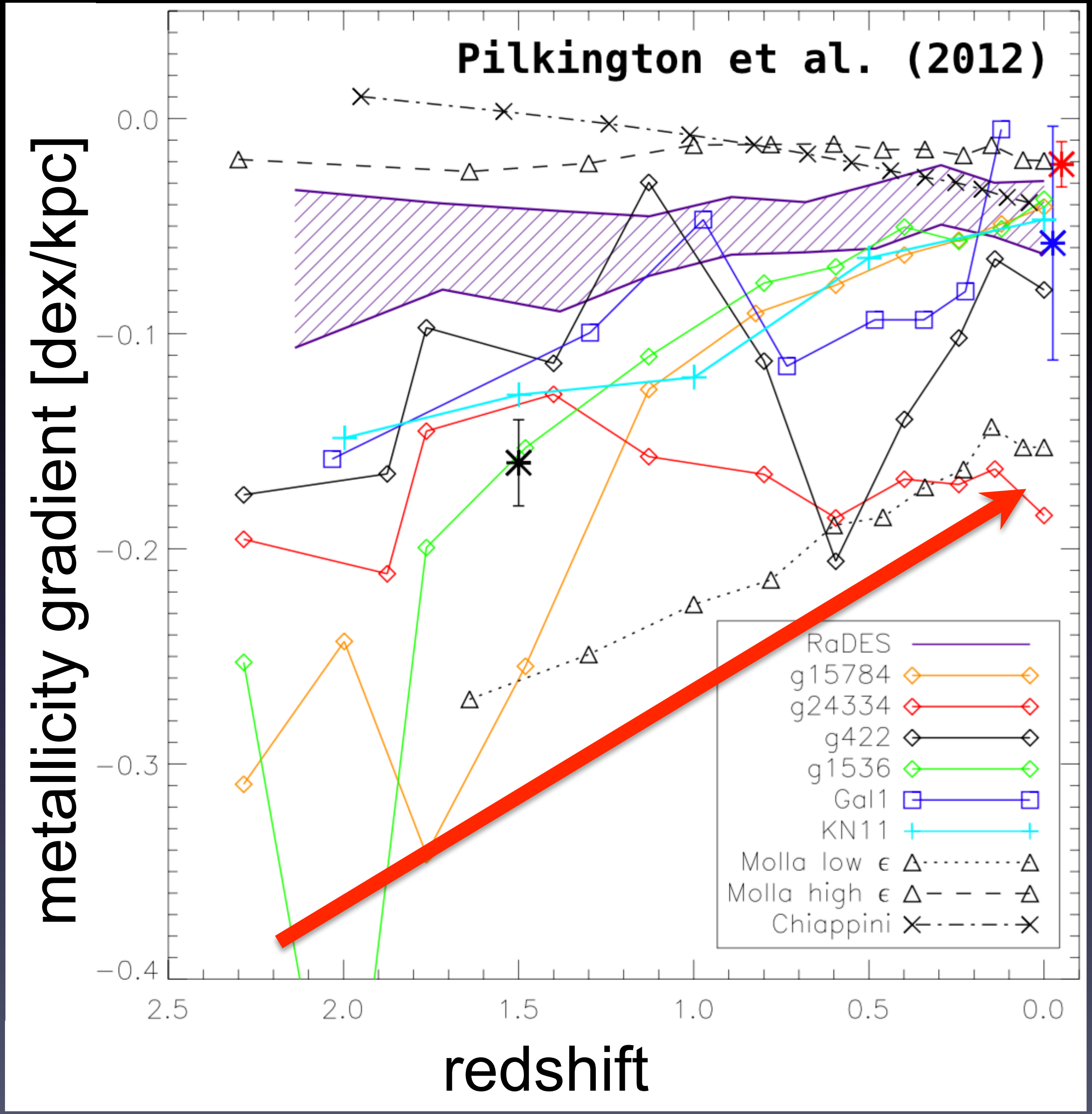

Discovery of strongly inverted metal gradients at high *z*

- analytical chemical evolution model of galaxy formation assuming inside-out growth predicts initially steep negative gradients flatten over time
- cosmological hydrodynamic simulations instead predict that metallicities are initially well mixed by strong feedback and later locked into a negative slope

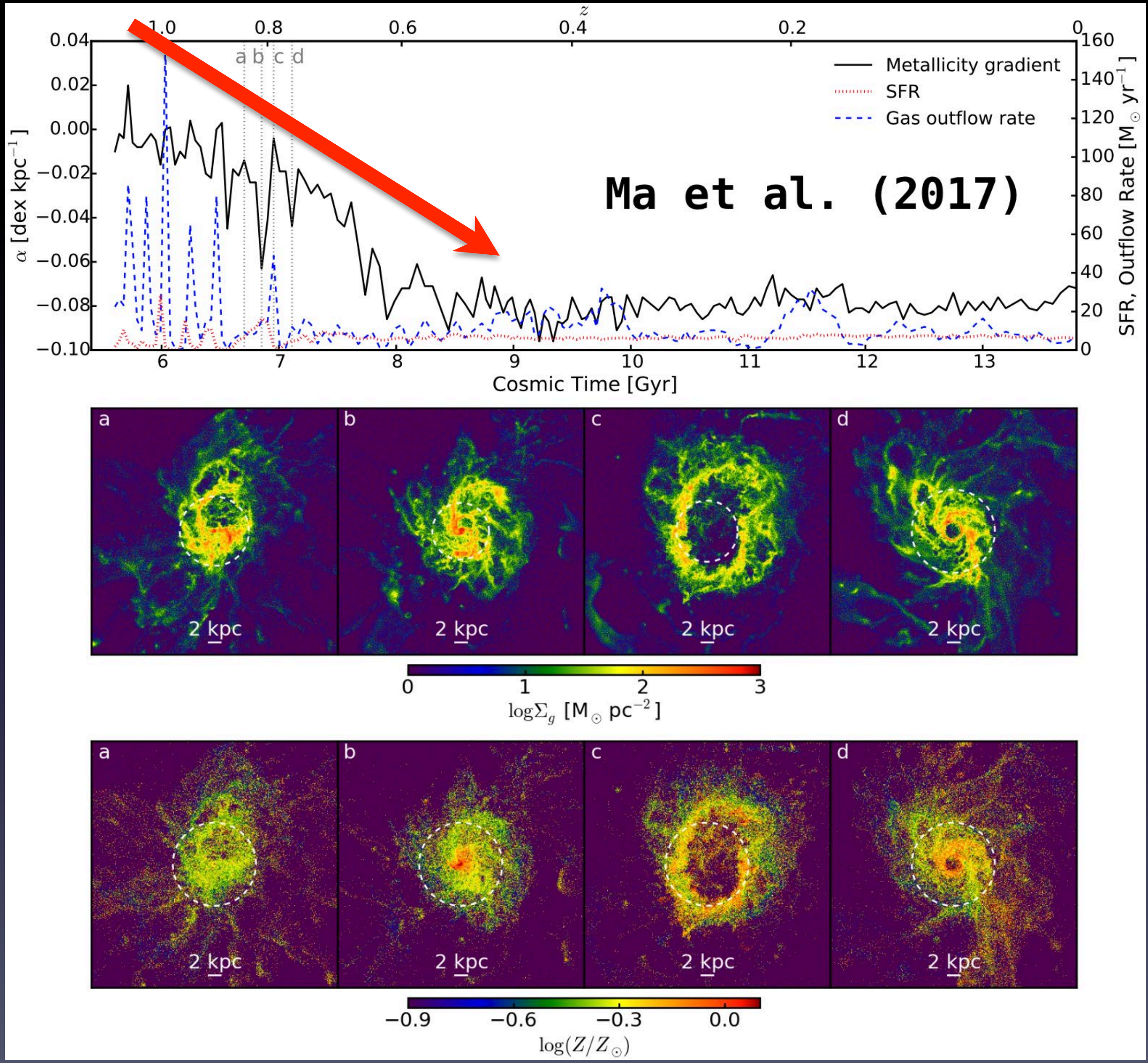

Discovery of strongly inverted metal gradients at high z

- analytical chemical evolution model of galaxy formation assuming inside-out growth predicts initially steep negative gradients flatten over time
- cosmological hydrodynamic simulations instead predict that metallicities are initially well mixed by strong feedback and later locked into a negative slope
- we obtained the first measurements with sub-kpc spatial resolution of strongly inverted (i.e. positive) metal gradients in dwarf galaxies

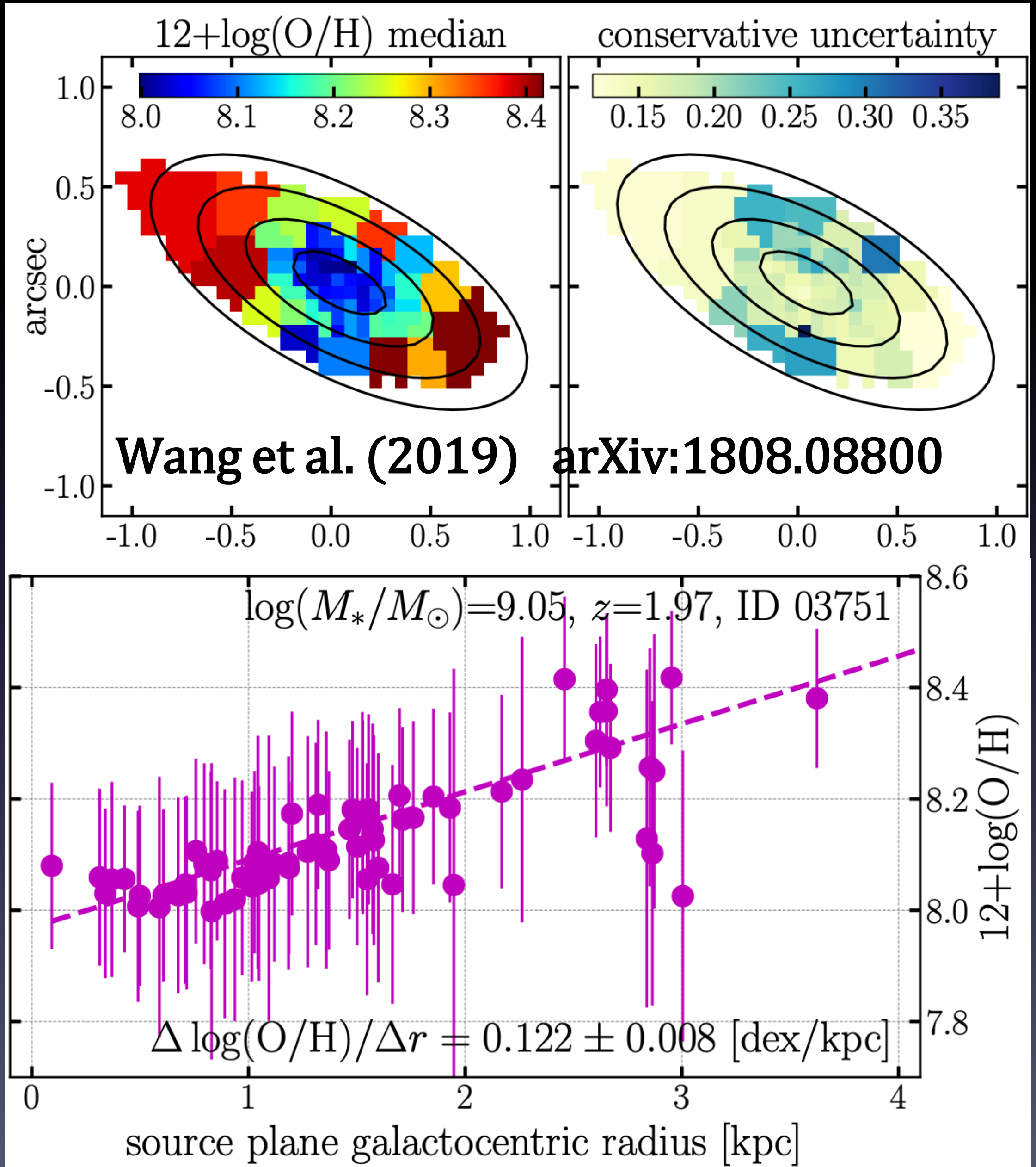

The reasons for galaxies showing inverted gradients

1. metal-enriched gas outflows triggered by powerful galactic winds that transport metals from galaxy center to outskirts

$$Z = Z_f \left[1 - \left(\frac{M_g}{M_i} \right)^{[f_i(1-z_i)-f_o(1-z_o)]/(\alpha - f_i + f_o)} \right]$$

Erb (2008) chemical evolution model

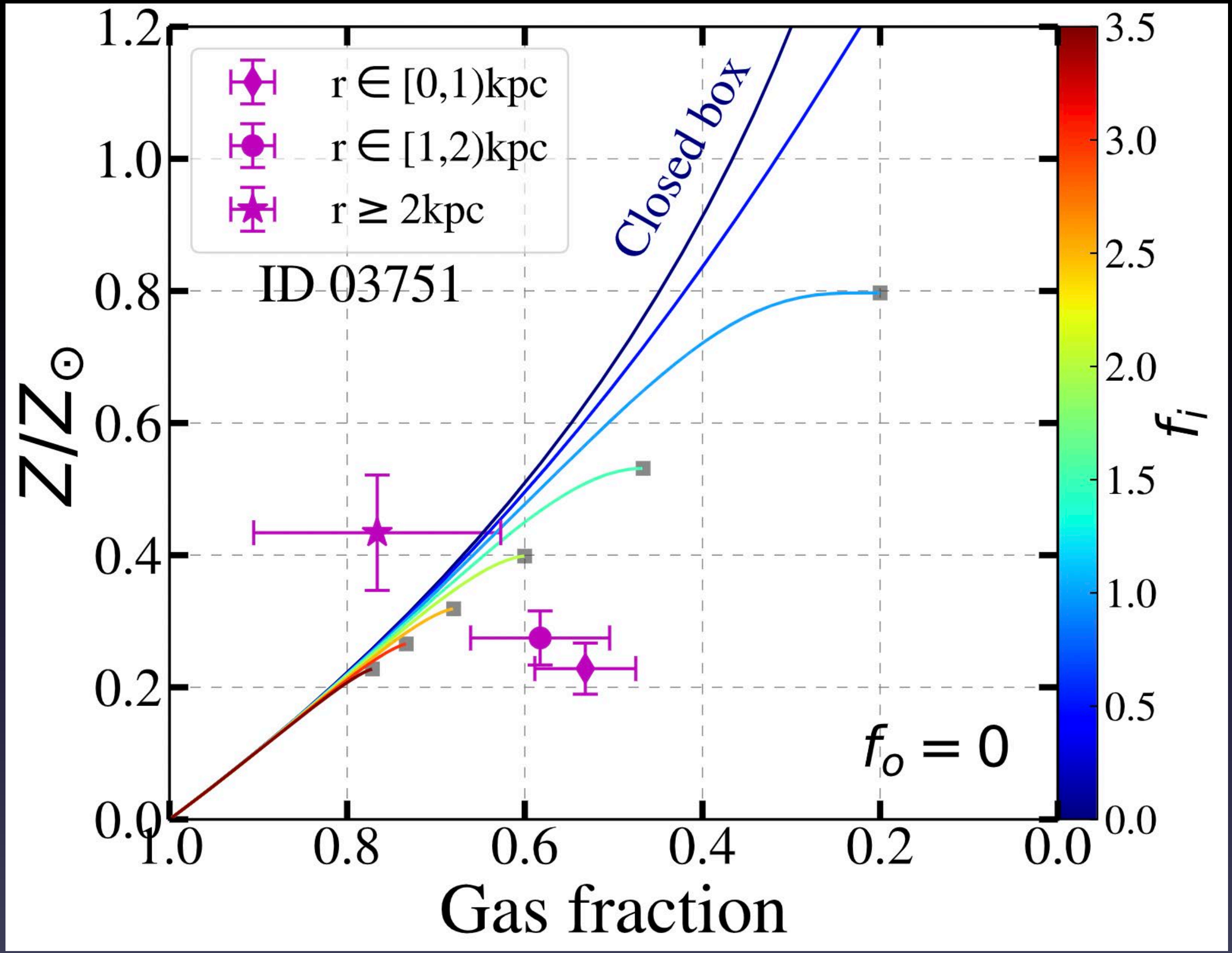

gas inflows alone cannot explain

The reasons for galaxies showing inverted gradients

1. metal-enriched gas outflows triggered by powerful galactic winds that transport metals from galaxy center to outskirts

$$Z_{\rm gas} = \left[Z_0 + y\tau_{\rm eq}\,\epsilon\left(1 - \exp\left(-\frac{t}{\tau_{\rm eq}}\right)\right)\right] \times \left[1 - \exp\left(\frac{-t/\tau_{\rm eq}}{1 - \exp(-t/\tau_{\rm eq})}\right)\right],$$

$$\tau_{\rm eq} = \frac{1}{\epsilon\,(1 - R + \lambda)}.$$

Peng & Maiolino (2014) chemical evolution model

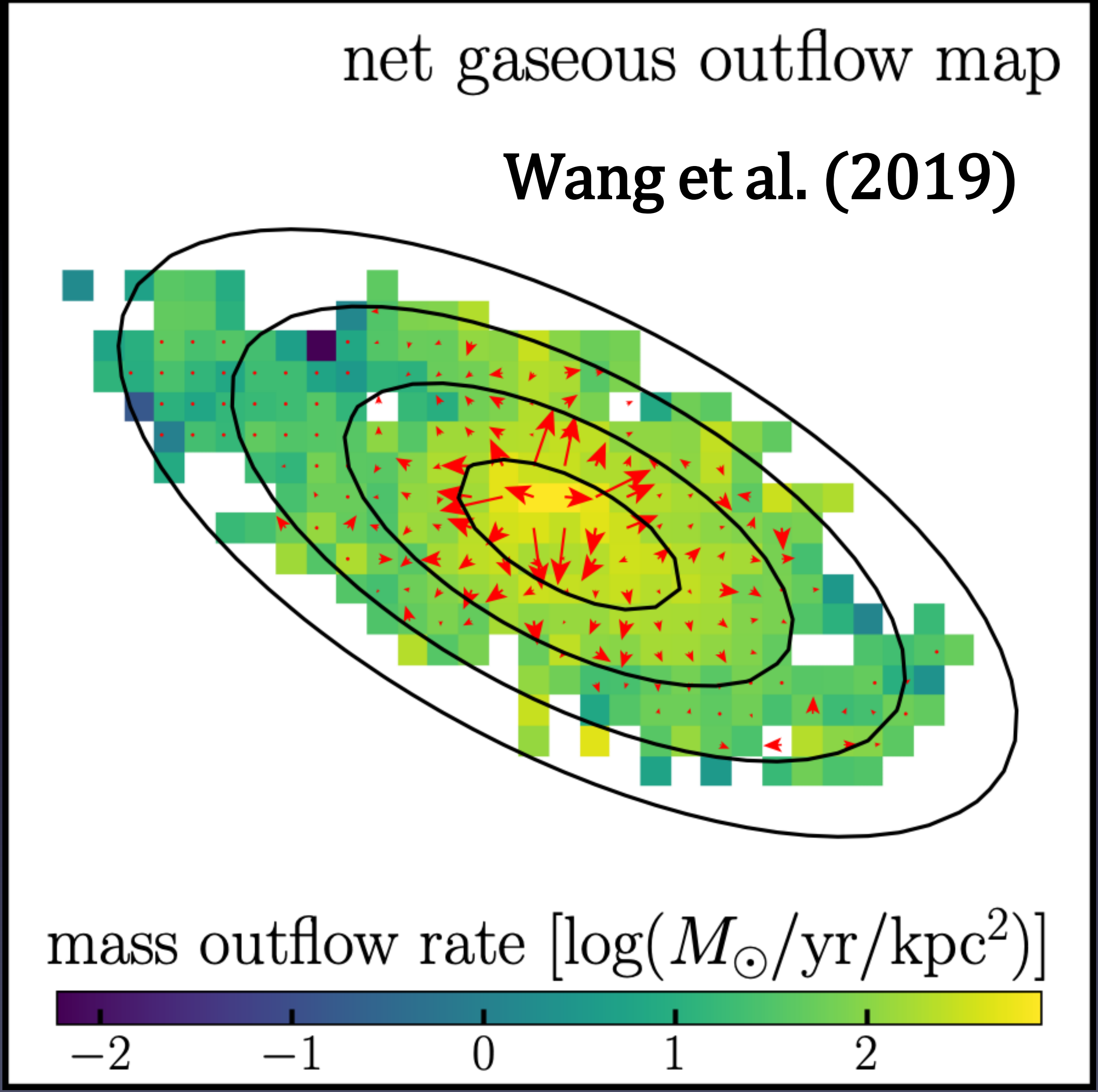

The reasons for galaxies showing inverted gradients

1. metal-enriched gas outflows triggered by powerful galactic winds that transport metals from galaxy center to outskirts
2. centrally-directed cold-mode gas accretion driven by the massive dark matter halos underlying galaxy protoclusters

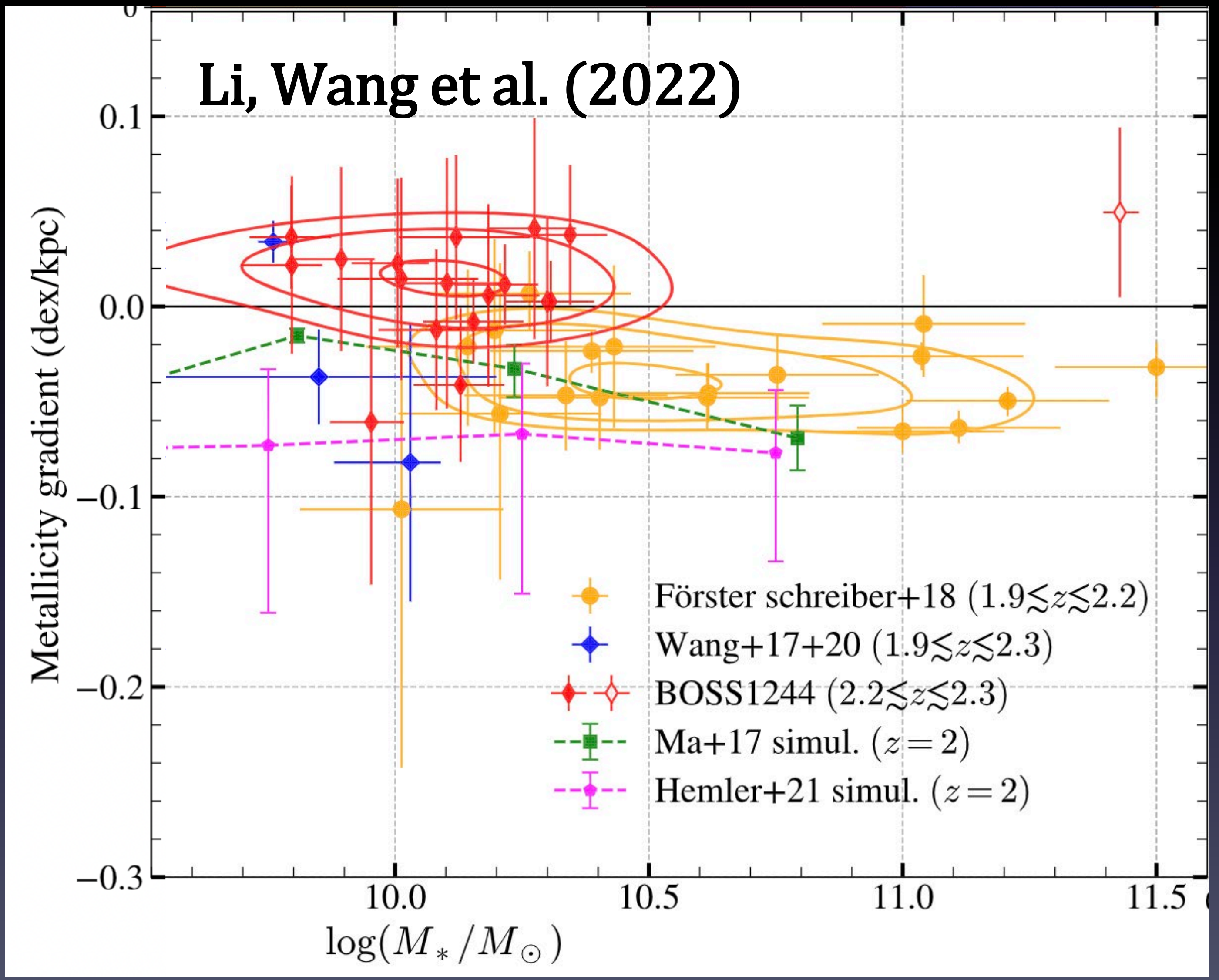

The reasons for galaxies showing inverted gradients

1. metal-enriched gas outflows triggered by powerful galactic winds that transport metals from galaxy center to outskirts
2. centrally-directed cold-mode gas accretion driven by the massive dark matter halos underlying galaxy protoclusters

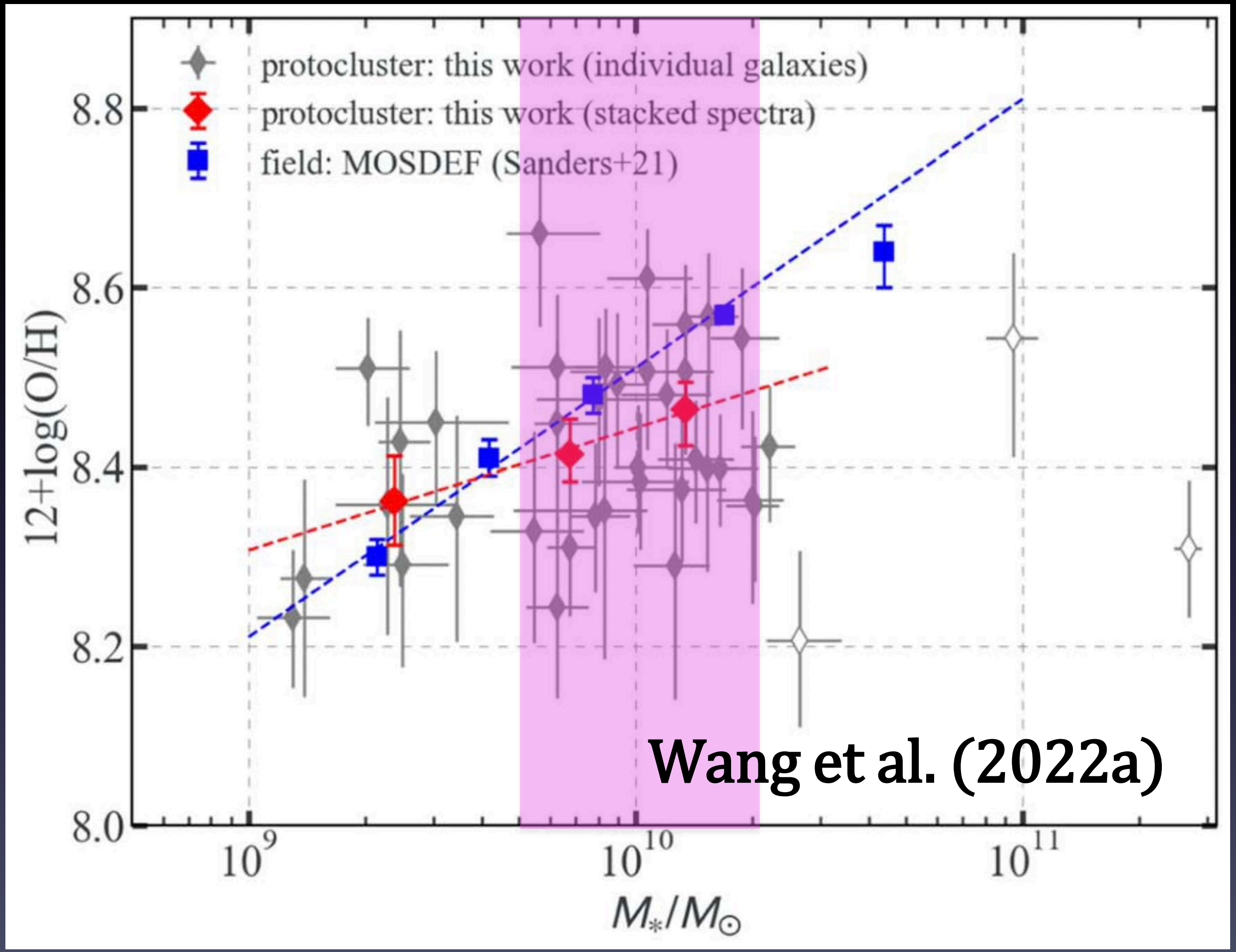

The reasons for galaxies showing inverted gradients

1. metal-enriched gas outflows triggered by powerful galactic winds that transport metals from galaxy center to outskirts
2. centrally-directed cold-mode gas accretion driven by the massive dark matter halos underlying galaxy protoclusters
3. metal-poor gas inflows to the inner galaxy disks induced by the strong tidal torques of close gravitational interactions